

Thermodynamics of polarization dynamics in ferroelectrics implemented by the phase field modelHaohua Wen^{1,2,3,4}, Jianyi Liu^{5,1,2,3}, Weijin Chen^{1,2,3,6,*}, Weiming Xiong^{1,2,3} and Yue Zheng^{1,2,3,†}¹*Guangdong Provincial Key Laboratory of Magnetoelectric Physics and Devices, School of Physics, Sun Yat-sen University, Guangzhou 510275, China*²*State Key Laboratory of Optoelectronic Materials and Technologies, School of Physics, Sun Yat-sen University, Guangzhou 510275, China*³*Centre for Physical Mechanics and Biophysics, School of Physics, Sun Yat-sen University, Guangzhou 510275, China*⁴*Sino-French Institute of Nuclear Engineering and Technology, Sun Yat-sen University, Zhuhai 519082, China*⁵*College of Physics, Qingdao University, Qingdao 266071, China*⁶*School of Materials, Sun Yat-sen University, Shenzhen 518107, China*

(Received 22 March 2022; revised 20 June 2022; accepted 18 July 2022; published 27 July 2022)

Polarization dynamical response is a fundamental issue for both physics and functional device applications for ferroelectrics. The phase field model has been proved as an efficient and indispensable method to capture the polarization evolution behaviors. With the size of polar element reducing to be atomic scale, the underlying physics in the phase field model should be well clarified. Starting from the generalized many-body stochastic dynamics, we discuss the thermodynamics of the polarization dynamics simulated based on the phase field scheme. It is found that the presence of random force guarantees the thermodynamics of polarization system. The numerical simulations indicate that the thermal fluctuations induced by random force give rise to a different heat dissipation mechanism during the process of polarization dynamical responses, which is not taken into account in the conventional phase field simulations. In addition, the thermal fluctuations of random force are found to lead to the unexpected phase instability when considering the atomic-scale polarization dynamical behaviors, which is considered to be originated from the incompatibility between the free-energy functional and random force used in the current phase field model. If simply revising the free-energy functional to get rid of such contradiction, the possible phase instability can be eliminated, but it results in the underestimation of thermal fluctuations and the associated polarization dynamical behaviors. In our opinion, the viable solution is to reconstruct the potential field, making it be compatible with the thermal fluctuation induced by random force. Our discussion could help to provide hints for the development of multiscale modeling scheme in polarization dynamics based on a phase field model.

DOI: [10.1103/PhysRevB.106.024111](https://doi.org/10.1103/PhysRevB.106.024111)**I. INTRODUCTION**

Polarization dynamical response in ferroelectrics under the external thermodynamic environment is an important issue for both fundamental physics and device applications [1–6]. Previous studies indicate that the macroscopic polarization responses observed in experiments are affected by multi-ingredients [7–9], like electric dipoles, ferroelectric domains, and space charges, etc. Dynamical responses of these ingredients lie on different spatial and temporal scales, so that polarization dynamics is a typical multiscale process, which the corresponding modeling methods are developed to study. For example, molecular dynamics [10–15] and effective Hamiltonian method [16–18] simulate the polarization dynamics in atomic scale, respectively, taking the ions and local modes as their collective representations of polarization. Using these atomistic methods, studies have been reported [10–18] to get the underlying physics of the

dynamics and thermodynamics in polarization dynamical responses in ferroelectric materials. On the other hand, based on Landau-Ginzburg-Devonshire (LGD) theory of ferroelectrics and the time-dependent Ginzburg-Landau (TDGL) equation, the phase field model (PFM) of ferroelectrics has been proven to be an efficient and indispensable method to yield the spatiotemporal profiles of ferroelectric domain evolution [19,20]. As a phenomenological simulation method, the physical picture of the conventional PFM scheme is more intuitive and the connection with the macroscopic thermodynamic theory is clear and well established [21], so that one can obtain the mechanical and thermodynamic characteristics consistent with the experimental observation. Recently, in order to study the high-frequency fluctuations of the microstructure in ferroelectrics, substantial progress has been made by extending PFM to capture the ultrafast polarization dynamics [22,23]. In this updated PFM simulation scheme, the inertial term of polarization dynamics is incorporated into the original TDGL equation to mimic the fluctuation behaviors under the applied external field. Besides, the ultrafast resonant coupling between ferroelectric and ferroelastic domain walls is considered instantaneously by introducing the dynamic equation of

*Corresponding author: chenweijin@mail.sysu.edu.cn

†Corresponding author: zhengy35@mail.sysu.edu.cn

mechanical deformation. In this scenario, the polarization dynamical responses might probably reduce to be atomic spatial and temporal scales. Applying PFM simulation scheme to the atomic scale, it requires to clarify the physical picture of polarization dynamics revealed in PFM simulations starting from the points of view of microdynamics and statistical thermodynamics. In particular, thermal fluctuations of polarization should be carefully taken into account [24], as well as the coupling between polarization and crystal dynamics in atomic spatiotemporal scale. In this paper, we aim to discuss the underlying physics of the current PFM simulation scheme in the cases of studying the polarization dynamics in the atomistic spatiotemporal response behaviors, so to give hints on the development of multiscale modeling.

This paper is organized as follows: The theoretical analysis about the stochastic nature of polarization dynamics in PFM scheme is proposed in Sec. II, where the random force (which is usually not taken into account) is proved to be the necessary condition to guarantee both the thermodynamics and dynamics of polarization system. In addition, the numerical PFM simulations in a defect-free BaTiO₃ (BTO) ferroelectric monodomain system are performed to verify the important role played by random force on polarization dynamics. In Sec. III, the incompatibility between the free-energy functional (or potential field) and the random force will give rise to the unexpected phase instability in current PFM scheme, and we will discuss the possible solution. The conclusion is drawn in Sec. IV.

II. STOCHASTIC NATURE OF POLARIZATION DYNAMICS IN PFM SCHEME

PFM is a phenomenological thermodynamic simulation method to study the spatial and temporal evolution of microstructure and the responses with respect to the external thermodynamic environment. It was developed on the basis of the continuum mass density functional theory, and the diffuse interface was adopted to describe the fluid interfaces [25]. Established on the LGD theory for ferroelectrics [26,27], PFM has now been an effective method to describe the polarization dynamics, where the temporal evolution of the polarization field $\mathbf{P}(\mathbf{r})$ is governed by the TDGL equation [27–29]

$$\dot{P}_\alpha = -L\delta_\alpha F + \xi_\alpha(\mathbf{r}, t) \quad \text{as } \alpha = x, y, z. \quad (1)$$

Here, L is the kinetic coefficient; $F = F[\mathbf{P}]$ is the free-energy functional, whose detail can be referred to Appendix A by taking the typical ferroelectric BTO as an example; $\delta_\alpha F \equiv \delta F / \delta P_\alpha$; and $\xi_\alpha(\mathbf{r}, t)$ is the Gaussian random force, satisfying [27–29]

$$\begin{cases} \langle \xi_\alpha(\mathbf{r}, t) \rangle = 0, \\ \langle \xi_\alpha(\mathbf{r}, t) \xi_\beta(\mathbf{r}', t') \rangle = \kappa \delta_{\alpha\beta} \delta(\mathbf{r} - \mathbf{r}') \delta(t - t') \end{cases} \quad (2)$$

with κ as the strength. Recently, in order to study the ultrafast polarization dynamical responses, an inertial term is introduced in the original TDGL equation of Eq. (1) [22,23], and the equation is written as

$$\mu' \ddot{P}_\alpha + \gamma' \dot{P}_\alpha + \delta_\alpha F = \xi'_\alpha(\mathbf{r}, t), \quad (3)$$

where μ' and γ' are the mass and damping coefficient of polarization evolution, respectively. ξ'_α is Gaussian random

force. In this paper, Eqs. (1) and (3) are named as first and second TDGL equations, respectively, governed by which the polarization dynamical systems are named Γ_1 and Γ_2 . In the following, we will present the important role played by random force on thermodynamics.

A. Discretized many-body polarization dynamics

Both variational TDGL equations of Eqs. (1) and (3) are usually nonlinear, which are solved numerically by adopting the finite-difference method, after meshing the continuous polarization field of $\mathbf{P}(\mathbf{r})$ into N cubic grids in the real space. The grid parameter is denoted by h in this paper, so that the cubic grid volume Ω is given by $\Omega = h^3$. Although this discretization operation is just a numerical approach, it significantly transfers the three-dimensional continuous polarization dynamics system to be a $3N$ -dimensional many-body stochastic one [30–32]: (1) the continuous space of $\mathbf{r} \in V$ maps to the discretized space of $\{\mathbf{r}_n\} \in V$ with $n = 1, 2, \dots, N$; (2) the continuous polarization field $\mathbf{P}(\mathbf{r})$ maps to a set of many-body discretized polarization field $\{P_{n,\alpha}\}$ as $\mathbf{P}(\mathbf{r}) \mapsto \{P_{n,\alpha}\}$, with $P_{n,\alpha} = P_\alpha(\mathbf{r}_n)$ denoting the α ($= x, y, z$) component of the n th grid polarization vector located at \mathbf{r}_n ; (3) the free-energy functional $F[\mathbf{P}]$ with the continuous polarization field as argument maps to the many-body thermodynamic potential function $U(\{P_{n,\alpha}\})$ with the discretized polarization field as variables, which is a function containing $3N$ degrees of freedom (DOF) defined in the phase space constructed by a complete basis set of $\{P_{n,\alpha}\}$. In this regard, the continuous first TDGL equation of Eq. (1) maps to a set of $3N$ discretized TDGL equations as

$$\dot{P}_i = -\gamma \partial_i U + \xi_i(t). \quad (4)$$

Here, P_i is equivalent to $P_{n,\alpha}$ denoting the DOF of the discretized polarization dynamics system with $i = 1, 2, \dots, 3N$; $\gamma = L/\Omega$; $U = U(\{P_{n,\alpha}\})$ is the potential force field, which makes $\partial_i U = \partial U / \partial P_i$ correspond to $\delta_\alpha F$ [30–33], and $\xi_i(t)$ is the Gaussian random force with $\langle \xi_i(t) \rangle = 0$ and $\langle \xi_i(t) \xi_j(t') \rangle = \kappa \delta_{ij} \delta(t - t')$. Similarly, the second TDGL equation of Eq. (3) maps to

$$\mu \ddot{P}_i = -\partial_i U - \gamma \dot{P}_i + \xi_i(t) \quad (5)$$

with $\mu = \Omega \mu'$, $\gamma = \Omega \gamma'$, and $\xi_i = \Omega \xi'_i$. The detail of the above discretization can be seen in Appendix B.

B. Dynamic equilibrium of polarization system and the stochastic environment

In a general microdynamic point of view, the total $3(N + M)$ DOF of a ferroelectric system can be divided into two categories: the $3N$ DOF representing the polarization dynamics directly, denoted by $\{P_i\}$, and the remaining $3M$ DOF, denoted by $\{x_j\}$ [30,31]. In this case, the Hamiltonian \mathcal{H} of the whole system can be written as

$$\mathcal{H}(\{P_i\}; \{x_j\}) = \mathcal{H}_P(\{P_i\}) + \mathcal{H}_x(\{x_j\}) + \mathcal{H}'. \quad (6)$$

Here, $\mathcal{H}_P(\{P_i\})$ and $\mathcal{H}_x(\{x_j\})$ denote the dynamics of $\{P_i\}$ and $\{x_j\}$, respectively, and \mathcal{H}' represents the interactions between $\{P_i\}$ and $\{x_j\}$. In general, the DOF of $\{x_j\}$ could be the atomic spins, electrons, mechanical strains, or even the so-called hard

modes, all of which do not represent the polarization dynamics directly. In particular, for a pure ferroelectrics system, \mathcal{H}_x describes the mechanical deformation dynamics, and \mathcal{H}' represents the electroelastic coupling. Note that, if $\mathcal{H}' = 0$, the dynamics of $\{x_j\}$ has no influence to that of $\{P_i\}$. Otherwise, the dynamics of $\{x_j\}$ will provide a thermodynamic environment for $\{P_i\}$, including the conservative and stochastic actions. On the one hand, the mean or instantaneous spatial configuration of $\{x_j\}$ would give rise to the conservative action on the dynamics of $\{P_i\}$ via \mathcal{H}' . This action can be absorbed into \mathcal{H}_P as $(\mathcal{H}_P + \mathcal{H}') \mapsto \mathcal{H}_P$. On the other hand, \mathcal{H}_x in Eq. (6) describes the thermal motions of $\{x_j\}$. It provides the stochastic action (denoted by \mathcal{H}_{env}) to the dynamics of $\{P_i\}$ [30,31], i.e., $\mathcal{H}_x \mapsto \mathcal{H}_{\text{env}}$. In principle, \mathcal{H}_{env} includes the fluctuation $\xi_i(t)$, and dissipation actions [i.e., $-\gamma \partial_i U$ in Eq. (4) and $-\gamma \dot{P}_i$ in Eq. (5)]. In this regard, the Hamiltonian \mathcal{H} of the polarization dynamical system in Eq. (6) can be thus rewritten as

$$\mathcal{H}(\{P_i\}; \{x_j\}) \mapsto \mathcal{H}(\{P_i\}; \eta) = \mathcal{H}_P(\{P_i\}) + \mathcal{H}_{\text{env}}(\eta). \quad (7)$$

Here, η is the fluctuation-dissipation ratio denoting the strength of the stochastic environment exerted by $\{P_i\}$, which is arising from the thermal motions of $\{x_j\}$. It should be reminded that it is a common way to separate the dynamics of different types of DOFs widely adopted in condensed matter theory.

In microdynamics, polarization dynamics between Γ_1 and Γ_2 are quite different, whose Hamiltonians are, respectively, written as

$$\begin{cases} \mathcal{H}_1 = U(\{P_i\}) + \mathcal{H}_{\text{env}}, & \text{for } \Gamma_1 \\ \mathcal{H}_2 = \sum_{i=1}^{3N} \frac{\mu}{2} \dot{P}_i^2 + U(\{P_i\}) + \mathcal{H}_{\text{env}}, & \text{for } \Gamma_2. \end{cases} \quad (8)$$

Accordingly, the first and second TDGL equations of Eqs. (4) and (5) are, respectively, the derived equations of motion for the microdynamic DOF of $\{P_i\}$ corresponding to the Hamiltonians of \mathcal{H}_1 and \mathcal{H}_2 defined in Eq. (8). Here, the potential force field U in \mathcal{H}_1 and \mathcal{H}_2 describes all the conservative actions exerted by $\{P_i\}$. It has the different form for the different ferroelectric system interested, for instance, it can be referred to Appendix A for the specific form used in BTO. As can be seen in the discussion presented in the subsequent sections, the specific form of U affects the evolution behaviors of polarization, which, however, does not bring the significant influence to the general thermodynamics. Therefore, it is not necessary to discuss the specific form of U in this section. Similarly, the stochastic actions \mathcal{H}_{env} provided by $\{x_j\}$ to $\{P_i\}$ can, in principle, be also expressed explicitly by introducing the instantaneous dynamical responses of $\{x_j\}$. However, except for bringing with the complexity of the mathematical form of \mathcal{H}_{env} in Eq. (6) or Eq. (7), it will not change the nature of physics. In this regard, when we focus on the polarization dynamics itself, the simplified form of Hamiltonian in Eq. (7) is appropriate and sufficient for us to discuss the microdynamics.

Note that the first and second TDGL equations of Eqs. (4) and (5) are the specific forms of the generalized Langevin equation, as

$$\dot{X}_i = \{X_i, \mathcal{H}\} - \gamma \partial_i \mathcal{H} + \xi_i(t), \quad (9)$$

which describes the stochastic microdynamics of a system including $3N$ DOF $\{X_i\}$. Here, $\{X_i, \mathcal{H}\}$ is the ‘‘Poisson bracket relation’’ and $\partial_i \mathcal{H} \equiv \partial \mathcal{H} / \partial X_i$. Choosing $X_i = P_i$ and $X_i = \mu \dot{P}_i$ in Eq. (9), the first and second TDGL equations can be respectively achieved with

$$\{P_i, \mathcal{H}_1\} = 0 \quad \text{and} \quad \{\mu \dot{P}_i, \mathcal{H}_2\} = -\partial_i U. \quad (10)$$

Due to the presence of random force ξ_i , the resulting phase-space trajectories of $\{P_i\}$ governed by either first or second TDGL equations are not deterministic but stochastic. Consequently, the phase-space probability distribution function $\varrho(t)$ is used to describe the stochastic nature of polarization dynamics, whose time-evolution behavior obeys the corresponding Fokker-Planck equation [30,31], i.e., for first TDGL equation of Γ_1 ,

$$\frac{\partial \varrho_1}{\partial t} = - \sum_i \frac{\partial}{\partial P_i} \left[\left(-\gamma \frac{\partial \mathcal{H}_1}{\partial P_i} \right) \varrho_1 \right] + \frac{\kappa}{2} \sum_i \frac{\partial^2 \varrho_1}{\partial P_i^2}, \quad (11)$$

and for second TDGL equation of Γ_2 ,

$$\begin{aligned} \frac{\partial \varrho_2}{\partial t} = & - \sum_i \frac{\partial}{\partial P_i} (\dot{P}_i \varrho_2) \\ & - \sum_i \frac{1}{\mu} \frac{\partial}{\partial \dot{P}_i} \left[\left(-\frac{\partial \mathcal{H}_2}{\partial P_i} - \frac{\gamma}{\mu} \frac{\partial \mathcal{H}_2}{\partial \dot{P}_i} \right) \varrho_2 \right] \\ & + \sum_i \frac{\kappa}{2\mu^2} \frac{\partial^2 \varrho_2}{\partial \dot{P}_i^2}. \end{aligned} \quad (12)$$

Polarization dynamical systems of Γ_1 and Γ_2 reach their own mechanical steady states at $t \rightarrow \infty$, so that $\partial \varrho_{1(2)} / \partial t = 0$. The equilibrium probability distribution $\varrho_{1(2)}$ then has the Boltzmann-type form as

$$\varrho_{1(2)} = C \exp(-\mathcal{H}_{1(2)}/\eta), \quad (13)$$

where C is a constant. Substituting Eq. (13) into (11) and (12) with $\partial \varrho_{1(2)} / \partial t = 0$, we have a unified expression as

$$\left(\frac{\kappa}{2\gamma} - \eta \right) \sum_{i=1}^{3N} (\eta \partial_i^2 \mathcal{H} - |\partial_i \mathcal{H}|^2) = 0. \quad (14)$$

The so-called fluctuation-dissipation relation (FDR) [34] can thus be achieved

$$\eta = \kappa/2\gamma \quad \text{and} \quad \eta = \langle |\partial_i \mathcal{H}|^2 \rangle / \langle \partial_i^2 \mathcal{H} \rangle, \quad (15)$$

where $\partial_i \mathcal{H} = \partial \mathcal{H} / \partial X_i$, $\partial_i^2 \mathcal{H} = \partial^2 \mathcal{H} / \partial X_i^2$, $\langle \dots \rangle$ is the ensemble average over the phase space constructed by $\{|X_i\}$, and $X_i = P_i$ for Γ_1 and $X_i = \mu \dot{P}_i$ for Γ_2 . In former expression of FDR in Eq. (15), η denotes the actions of the stochastic mechanical environment as $\kappa/2\gamma$, which is the strength of thermal motions of $\{x_j\}$. Although η is independent of the dynamics of system interested, it determines the stochastic nature of the microdynamic system as presented in the latter expression of FDR in Eq. (15). This intrinsic stochastic connection can also be seen in the expression of ϱ in Eq. (13) indexed by η , which indicates the dynamical equilibrium between the microdynamic system and its stochastic environment. As addressed in Ref. [34], if one cannot define the relation between η and the thermodynamic temperature T , the thermodynamics of the above-mentioned microdynamic

system cannot be well defined. Therefore, we have to establish the thermodynamic relation in terms of $\eta = \eta(T) = \langle |\partial_i \mathcal{H}|^2 \rangle / \langle \partial_i^2 \mathcal{H} \rangle$ in accordance with Eq. (15).

C. Zeroth law of thermodynamics

For the specific ferroelectric system, as addressed in Eq. (15), the thermal motions of $\{x_j\}$ and $\{P_i\}$ at finite temperatures, respectively, characterized by $\kappa/2\gamma$ and $\langle |\partial_i \mathcal{H}|^2 \rangle / \langle \partial_i^2 \mathcal{H} \rangle$, carry out the mechanical momentum and energy exchange continuously to guarantee the dynamical equilibration of the whole system. On the one hand, for the dynamics of $\{P_i\}$, the stochastic mechanical actions of \mathcal{H}_{env} in Eq. (8) characterized by $\eta = \kappa/2\gamma$ are in fact arising from the thermal motions of $\{x_j\}$ with strength denoted by $\eta = k_B T_x$ (T_x is the thermodynamic temperature of $\{x_j\}$) [34], so that

$$\kappa/2\gamma = \eta = k_B T_x. \quad (16)$$

On the other hand, according to statistical thermodynamics, the thermodynamic temperature T_P of polarization dynamical system Γ_1 and Γ_2 are, respectively, given by

$$\begin{cases} k_B T_P = \frac{\langle |\partial_i \mathcal{H}|^2 \rangle}{\langle \partial_i^2 \mathcal{H} \rangle} = \frac{\langle |\partial_i U|^2 \rangle}{\langle \partial_i^2 U \rangle}, & \text{for } \Gamma_1 \\ = \langle \mu \dot{P}_i^2 \rangle, & \text{for } \Gamma_2 \end{cases} \quad (17)$$

which are consistent with the equipartition and conjugate variables theorem (or named hypervirial) [35–40] (see detail in Appendix C). Combining Eqs. (15)–(17), we can arrive at the thermodynamic zeroth law of polarization dynamics, i.e.,

$$T_x = \eta/k_B = T_P \quad (18)$$

which is written in terms of

$$\begin{cases} \frac{\kappa}{2\gamma} = k_B T = \frac{\langle |\partial_i U|^2 \rangle}{\langle \partial_i^2 U \rangle}, & \text{for } \Gamma_1 \\ = \langle \mu \dot{P}_i^2 \rangle, & \text{for } \Gamma_2 \end{cases} \quad (19)$$

with $T = T_x = T_P$. Here, the thermodynamic temperature T is a parameter characterizing the stochastic actions of the Langevin heat bath as $k_B T = k_B T_x = \kappa/2\gamma$, and a thermodynamic observable function of the dynamical phase-space trajectory $\{P_i\}$ as $k_B T = k_B T_P = \langle |\partial_i U|^2 \rangle / \langle \partial_i^2 U \rangle$ for Γ_1 and $k_B T_P = \langle \mu \dot{P}_i^2 \rangle$ for Γ_2 .

As known, temperature is a thermodynamic concept, which is well defined under the equilibrium states, so that one should be careful to apply it to a nonequilibrium polarization configuration. However, under the local equilibrium assumption [41,42], e.g., in the cases where the local equilibration processes are much faster than the global energy exchange rate, the polarization temperature can still be well defined in terms of a local set of dynamical variables following Eq. (19), and the thermodynamic zeroth law can be well satisfied at arbitrary instant during the polarization relaxation process.

D. Discussion

It can be seen from the above analysis, the presence of the random force, either $\xi_\alpha(\mathbf{r}, t)$ in Eqs. (1) and (3) or $\xi_i(t)$ in

Eqs. (4) and (5), gives rise to the stochastic nature of the polarization dynamics, which, together with the dissipation actions, guarantees the correctness of thermodynamics of polarization dynamical system.

Note that the random force was involved in the original TDGL equation to account for the temperature effects, either for the issues about structural phase transition in crystalline solids and other phase transformation phenomena [30,31] or ferroelectric polarization dynamics [27–29]. However, the random force is usually eliminated in the PFM scheme used currently for polarization dynamics, where the temperature effects are alternatively taken into account by treating T as a thermodynamic parameter involved in the expression of free-energy functional $F(T)$ or potential force field $U(T)$ [20,21]. It should be reminded that the temperature effects arising from random force are quite different from those induced by $U(T)$ [24]: (1) when $\xi_i(t) \neq 0$, the random force can give rise to the corresponding thermal fluctuations of polarization dynamics around its equilibrium state; (2) taking temperature T as a parameter involved in $F(T)$ or $U(T)$ with $\xi_i(t) = 0$, it just results in temperature-dependent conservative force $\partial_i U(T)$, thus giving rise to the change of equilibrium state as temperature changes.

In general cases, the equilibrium state of polarization in a ferroelectric system is determined by the free-energy functional F or potential force field U , so that the equilibrium behavior of polarization dynamics can be also well reproduced, if setting $\xi_i(t) = 0$ in both first and second TDGL equations. In particular, for the issues of polarization responses can be regarded as quasistatic approximately, the thermal fluctuations induced by $\xi_i(t)$ do not play the predominant roles on the microstructural evolution of the polarization dynamics [20,28,29]. In this case, the temperature effects can be well described by the temperature dependence of free-energy functional or potential force field, without effects of random force. However, when we consider the ultrafast polarization dynamics related to the atomic spatiotemporal evolution behaviors, e.g., the dynamics of nanosize domain-wall structure, the high-frequency fluctuation information has to be involved. In fact, the second TDGL equation with $\xi_i(t) = 0$ as the extension of first TDGL equation by adding an inertial term, equivalent to the nonlinear Klein-Gordon equation, aims to obtain the polarization fluctuations [22,43]. Nevertheless, lacking the random force, the thermal fluctuations will vanish after the system reaches its equilibrium state, and the thermodynamics zeroth law cannot be guaranteed. In other words, effects of the inertial term and random force are quite different. Before equilibrium, the inertial term can give rise to the thermal vibrations of observed total polarization, indicating the energetic exchange between the kinetic ($\frac{1}{2}\mu\dot{P}^2$) and potential energies ($U(P)$). However, the vibration amplitude decays with time elapsed and finally vanishes under equilibrium because of the dissipation action provided by the term of $-\gamma\dot{P}$. In this case, the thermodynamic temperature of the system cannot be balanced with the external thermodynamic environment [e.g., see the results of case I plotted in Fig. 3(d) or 3(f)]. Otherwise, similar fluctuation behaviors will always be present induced by the effects of random force. Therefore, effects of inertial term and random force are not the simple accumulation. From this point of view, the random

force should not be eliminated in both first and second TDGL equations when we study the ultrafast polarization dynamics at atomic spatiotemporal scale (see detail in Appendix D).

Let us analyze this issue in another point of view. As a phenomenological simulation method, the viable and direct way to examine the rationality and reliability is to compare simulation results and the experimental observations. For PFM simulations of polarization dynamics, the time evolution of the global $P_\alpha(t)$ or local polarization $P_\alpha(\mathbf{r}, t)$ is the key quantity characterizing the evolution of the interested polarization system. After discretization operation, $P_\alpha(t)$ is estimated as the ensemble average of all grid polarizations as

$$P_\alpha(t) = \langle P_{n,\alpha}(t) \rangle = \int P_{n,\alpha} \varrho d^N P_{n,\alpha}, \quad (20)$$

where $\varrho = \varrho(\{P_{n,\alpha}(t)\})$ is the state probability distribution function of the system for a given polarization configuration $\{P_{n,\alpha}\}$. A large number of practices have proved that PFM simulations based on the TDGL equation without random force can obtain the accurate mathematical expectation $P_\alpha(t)$ of polarization dynamics (e.g., see the review paper [20]). Note that just ensuring the accuracy of polarization observed $P_\alpha(t)$ cannot guarantee the self-consistency of thermodynamics. According to the fluctuation theorem, even staying at equilibrium states, there is thermal fluctuation for each thermodynamic observable quantity, e.g., $\langle P_{n,\alpha}^2 \rangle \neq 0$. Therefore, the high-order statistical moments of ϱ should be obtained to achieve the thermodynamic quantities concerned, as well as the dynamical behaviors of polarization. Readers can see the detailed analysis in Appendix D. In the following, we will perform the PFM simulations on polarization dynamics by taking BTO as an example, to show the indispensable role played by the random force on both the thermodynamics and dynamics of polarization.

E. Numerical verification

For clarity and without loss of generality, we consider the system having a single ferroelectric domain, e.g., a stress-free perfect BTO crystal with periodic boundary condition applied. Figure 1 illustrates the typical biased double-well potential force field $U(P)$ as function of macroscopic polarization P . Here, P_A and P_B are, respectively, two local equilibrium states, separated by an energy barrier U_m with P_C as the saddle-point state. Note that P in fact is the phase-space coordinate representing the polarization configuration as $P \equiv \{P_i\}$ evolving upon the given potential force field $U(P)$. Applying the external field will modify the feature of $U(P)$, so to affect the polarization dynamics. As addressed in Ref. [15], there are two typical processes for polarization dynamics: (1) the relaxation process from an excited state P_e to the nearest equilibrium state P_A spontaneously; (2) the reversal switching process from one equilibrium state P_A to another one P_B under an applied external field and thermal assistance. In the following, we will perform PFM simulations for these two typical polarization dynamical processes to show the role played by random force on polarization thermodynamics and dynamics, which are respectively plotted in Figs. 2 and 3.

In our PFM simulations for both processes of polarization dynamics, the simulation system is discretized into

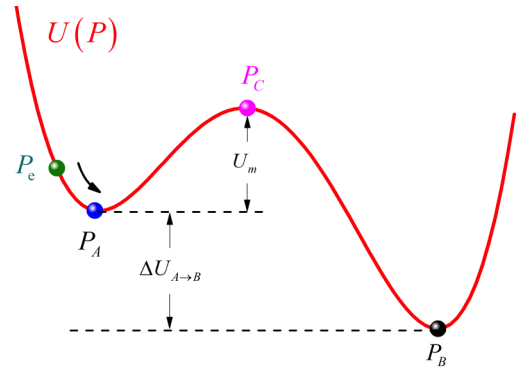


FIG. 1. The schematics of a typical biased double-well potential force field $U(P)$ as function of total polarization P . Here, P is the phase-space coordinate denoting the states of a many-body stochastic polarization dynamical system $\{P_i\}$. P_A and P_B are two local equilibrium states separated by a barrier U_m with P_C as the saddle-point state. In principle, there are two typical polarization dynamical responses: (1) the relaxation process from an excited state P_e to the nearest equilibrium state P_A ; (2) the switching process from P_A to P_B under the external stimulation.

$64h \times 64h \times 64h$ grids with $h = 4.0$ nm, which is embedded in the Langevin heat bath of $T_x = 300$ K. The phase-space trajectories $\{P_{n,\alpha}(t)\}$ are obtained by solving the TDGL equation, where all the parameters can be referred to Refs. [44,45] (see detail in Appendix A). The first [i.e., Eq. (4)] and second TDGL [i.e., Eq. (5)] equations are solved via an explicit Euler method with a time step of 1 fs, and the FFT approach is adopted to calculate the conservative force in TDGL equation [28,29,45]. The total polarization $P_\alpha(t)$ of the systems considered is thus thermodynamic observable as $P_\alpha = \langle P_{n,\alpha} \rangle$. Doubling the numbers of meshing grids and decreasing the time step are examined to result in the statistical error less than $\sim 0.1\%$. The FFT simulations are performed by a self-developed C language code, with the use of the C subroutine library FFTW for computing the discrete Fourier transform and the standard software library CLAPACK for numerical linear algebra.

BTO is a typical ferroelectric material, presenting a tetragonal (T) phase at $T = 300$ K with spontaneous polarization along the z direction, i.e., $|P_z| = P_0$ (≈ 0.26 C/m²). In PFM simulations, a double-well potential field U is designed for each $P_{n,z}$, including two equivalent minima at $P_{n,z} = \pm P_0$ separated by an energy barrier U_m , as plotted as in Fig. 2(a). The time-evolution behaviors of P_α are plotted in Figs. 2(c) and 2(d), which well indicates the feature of a T phase in BTO as $P_x = P_y \approx 0$ and $P_z \approx P_0$ at $t > 5$ ps. The probability distribution of P_α given in Fig. 2(e) also demonstrates the thermal fluctuations under equilibrium induced by the random force. In addition, the distribution of P_z is not symmetrical around P_0 . Because the potential field U around the potential well at P_0 is asymmetrically shown in Fig. 2(a) and the presence of random force makes the system feel the neighborhood of the potential well, the probability for $P_{n,z} \leq P_0(1-s)$ is larger than that for $P_{n,z} \geq P_0(1+s)$, where s is an arbitrary small value. Therefore, there is slight offset of P_z from P_0 , as $P_z \approx 0.99P_0$ shown in Fig. 2(d). This is a typical anharmonic effect, as well as a thermodynamic phenomenon, showing

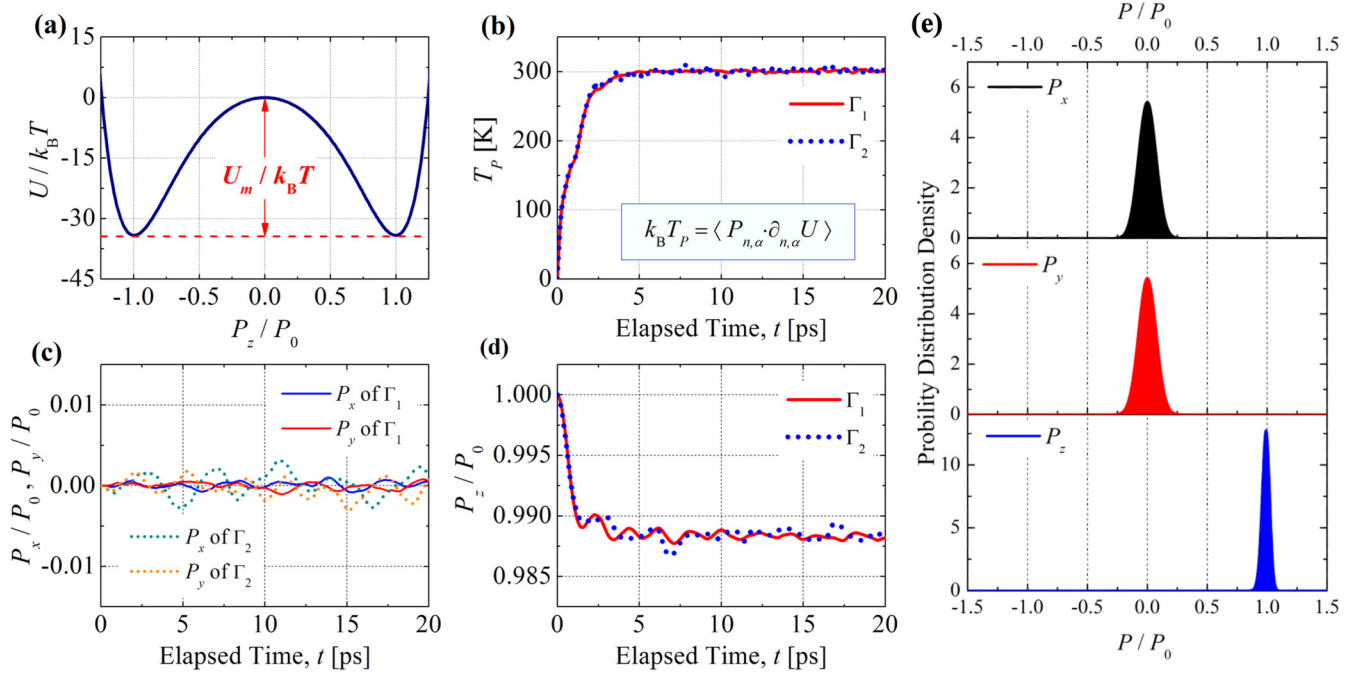


FIG. 2. The PFM simulation results of polarization relaxation process from P_e to P_A illustrated in Fig. 1, in the case of BTO at 300 K with $h = 4.0$ nm. (a) The potential landscape U along P_z . (b) The estimated polarization temperature T_p following Eq. (19) (see detail in Appendix C). (c), (d) The time-evolution behaviors of P_α with $\alpha = x, y, z$. (e) The probability density of P_α under equilibrium. Here, Γ_1 and Γ_2 are the polarization dynamical systems governed by first and second TDGL equations, respectively.

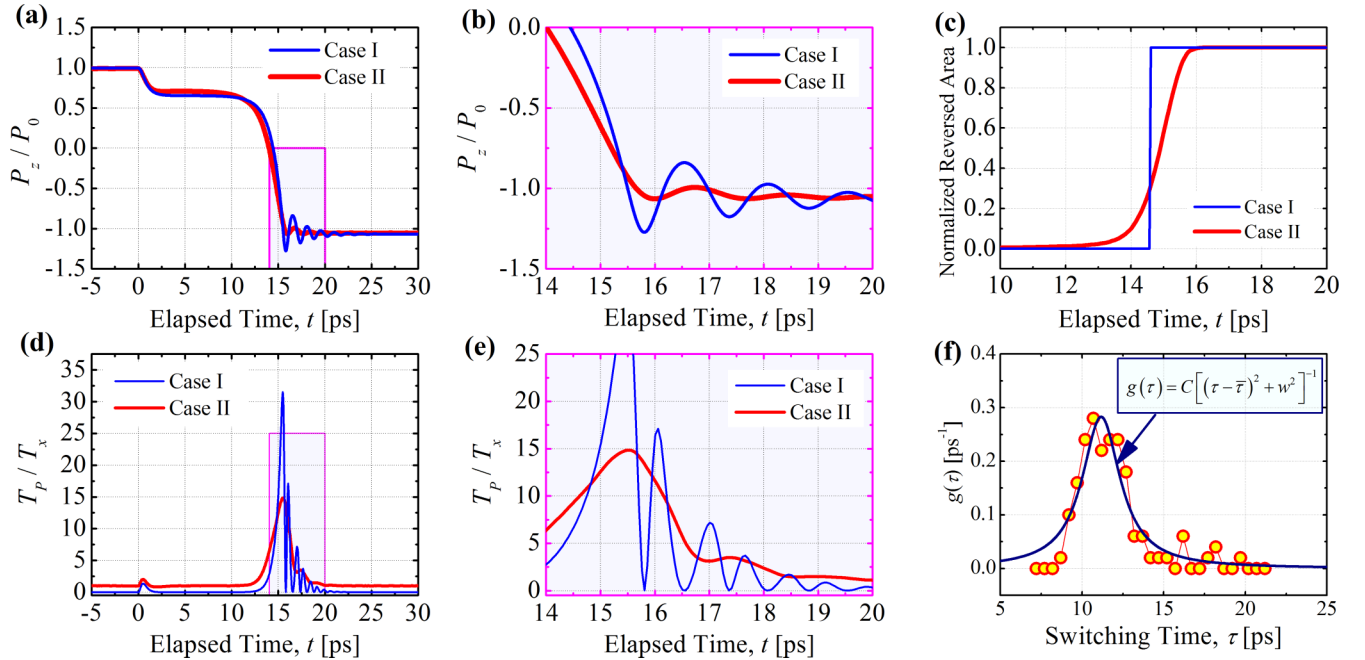


FIG. 3. The results of polarization reversal switching process from P_A to P_B illustrated in Fig. 1, in the case of BTO at 300 K with $h = 4.0$ nm. Here, the polarization switching under the applied reversal $E_{\text{ext}} = -1.41 \times 10^7$ V/m is simulated based on second TDGL equations without and with the presence of random force in Eq. (21), which is named case I and II, respectively. (a) The time evolution of P_z , and (b) the enlarged detail; (c) the time-dependent normalized reversed area; (d) the time evolution of polarization temperature estimated by $k_B T_p = \langle \mu \dot{P}_i^2 \rangle$, and (e) the enlarged detail; (f) the statistics of switching time τ of case II with the random force involved, which well follows the Lorentzian distribution shown in Eq. (22).

the significance of random force to the thermodynamics. Correspondingly, the polarization temperature T_p , estimated following the conjugated coordinates theorem [35–40] as $k_B T_p = \langle P_{n,\alpha} \partial_{n,\alpha} U \rangle$ (see detail in Appendix C), gradually increases to be the temperature T_x of the thermal heat bath, so to confirm the equivalent relation of the thermodynamics zeroth law expressed in Eqs. (18) and (19). In this regard, the thermodynamics of polarization can be achieved, and both first and second TDGL equations can govern the same behaviors for polarization dynamics. It is obvious that if setting $\xi_{n,\alpha}(t) = 0$ in both first or second TDGL equations, the fluctuation shown in Fig. 2 cannot be observed when the system is under equilibrium, although it can lead to the correct equilibrium state of polarization dynamics.

Applying a sufficient large reversal external electric field E_{ext} on a ferroelectric domain with nonzero spontaneous polarization leads to the polarization switching [15]. Performing the PFM simulation without the thermal assistance by setting $\xi_i(t) = 0$ in second TDGL equation of Eq. (5), the polarization switching occurs for a monodomain structure in the case of $|E_{\text{ext}}| > E_{\text{crit}}$ (E_{crit} is the thermodynamic coercive field [15,46]). However, if setting $\xi_i(t) \neq 0$ in second TDGL equation of Eq. (5), the polarization switching can occur for a monodomain structure even in the case of $|E_{\text{ext}}|$ is smaller than E_{crit} due to the thermal fluctuations.

The polarization dynamics under the applied reversal E_{ext} on the monodomain structure of BTO is simulated based on second TDGL equations with $\xi_i(t) = 0$ and $\xi_i(t) \neq 0$, respectively, which are named case I and II, as

$$\begin{cases} \mu \ddot{P}_i + \gamma \dot{P}_i + \partial_i U = 0, & \text{for case I} \\ \mu \ddot{P}_i + \gamma \dot{P}_i + \partial_i U = \xi_i(t), & \text{for case II.} \end{cases} \quad (21)$$

The simulation system is discretized into grids with size of $h = 4.0$ nm. Here, the system is first relaxed at its equilibrium states with $P_z = P_0$ at $T = 300$ K. Figure 3 plots the simulation results. In Fig. 3(a), $E_{\text{ext}} = -1.41 \times 10^7$ V/m is applied at the moment of $t = 0$, under which the value of P_z starts to decrease to be $P_z = 0.7P_0$ at $2.5 < t < 10.0$ ps, and then rapidly reduces and reaches the value of $-P_0$ at $t \sim 20$ ps. Similar time-evolution behaviors of $P_z(t)$ are revealed in both cases I and II. The difference is the fluctuation of $P_z(t)$ when the switching finishes at $15 < t < 20$ ps, as demonstrated in the enlarged figure of Fig. 3(b). For case I, P_z evolves like a typical damped oscillator without effects of random force. Otherwise, such behavior is not so significant for case II. In addition, the time-dependent normalized reversed area plotted in Fig. 3(c) further indicates the effects of $\xi_i(t)$. For case I without thermal assistance induced by $\xi_i(t)$, the polarization at each grid $P_{n,\alpha}$ uniformly decreases, so that they finish the switching process suddenly at the moment of $t \sim 14.5$ ps. However, for case II, the grid polarization $P_{n,\alpha}$ reversal occurs randomly with the thermal fluctuation, resulting in the so-called local nucleation and the gradual rise of the normalized reversed area with time elapsed shown in Fig. 3(c). In this case, the switching time τ is not deterministic, whose stochastic feature can be described by a Lorentzian distribution as [47]

$$g(\tau) = C[(\tau - \bar{\tau})^2 + w^2]^{-1}, \quad (22)$$

where $\bar{\tau}$ is the mean value of τ , w is the half-width, and C is a constant. Here, τ is defined as the time duration for P_z reducing from P_0 to 0, and the distribution of τ shown in Fig. 3(f) is obtained by frequency counting from 100 independent simulations of polarization switching, which is found to well satisfy the expected Lorentzian distribution in Eq. (22). Note that the similar behavior of τ cannot be found in case I without effects of random force. Furthermore, as illustrated in Figs. 3(d) and 3(e), the polarization temperature T_p (estimated following $k_B T_p = \langle \mu \dot{P}_i^2 \rangle$) can be well described for case II far away from the switching process. For both cases I and II, there are small peaks of T_p at the moment of $t = 0$ when applying E_{ext} to the system because $P_z = P_0$ is not a stable state under the actions of E_{ext} , so that it will relax to the new state accompanied with heat dissipation. For the same reason, T_p shows the larger rises subsequently during the fast reversal processes at $12 < t < 16$ ps. The decay of T_p with oscillation at $t > 16$ ps is induced by the inertial term of $\mu \dot{P}_i$ in Eq. (21), during which, however, the heat dissipates faster in case II with the help of random force. That is because the heat dissipation mechanisms are different between case I and II. Take the polarization switching under the applied E_{ext} for example. For the ferroelectric system considered, the action of E_{ext} is the work done, which leads to the increase of internal energy stored in polarization system, and the heat dissipation. For case I, without effects of random force, the heat dissipates to its environment via the dissipation actions provided by the $-\gamma \dot{P}_i$, which is the heat transfer from the system to its environment. However, the participation of random force $\xi_i(t)$ provides a feedback of the heat exchange from its environment to the system interested. From this thermodynamic point of view, the presence of random force is a necessary condition to model the full thermodynamic actions.

To sum up, the thermal fluctuations induced by the random force have the non-negligible effects on polarization dynamics, which, on the one hand, guarantee the thermodynamics, i.e., the thermodynamic zeroth law, as demonstrated as the polarization relaxation process in Fig. 2, on the other hand, give rise to a different polarization dynamical behavior as indicated as the polarization switching process in Fig. 3.

III. INCOMPATIBILITY OF CURRENT PFM SCHEME

A. Phase instability

From the PFM simulation results plotted in Figs. 2 and 3, both the thermodynamics and dynamics can be achieved instantaneously based on the stochastic TDGL equation with $\xi_i(t) \neq 0$. However, the discretized grid size of $h = 4.0$ nm is too large, and not suitable for modeling the dynamics of ferroelectric domain structure and domain-wall motion. For the typical ferroelectric materials, the width of domain wall is around 2 nm. In order to ensure the spatial resolution of diffuse interface used in PFM scheme, the meshing-grid size h should be less than 1 nm. In practice, the grid discretization of $h = 0.4$ nm is widely adopted in PFM simulations of polarization dynamics [48–50]. In principle, PFM simulations results of polarization dynamics will not rely on the discretized grid size. However, as a phenomenological approach developed on the basis of the continuum mechanics

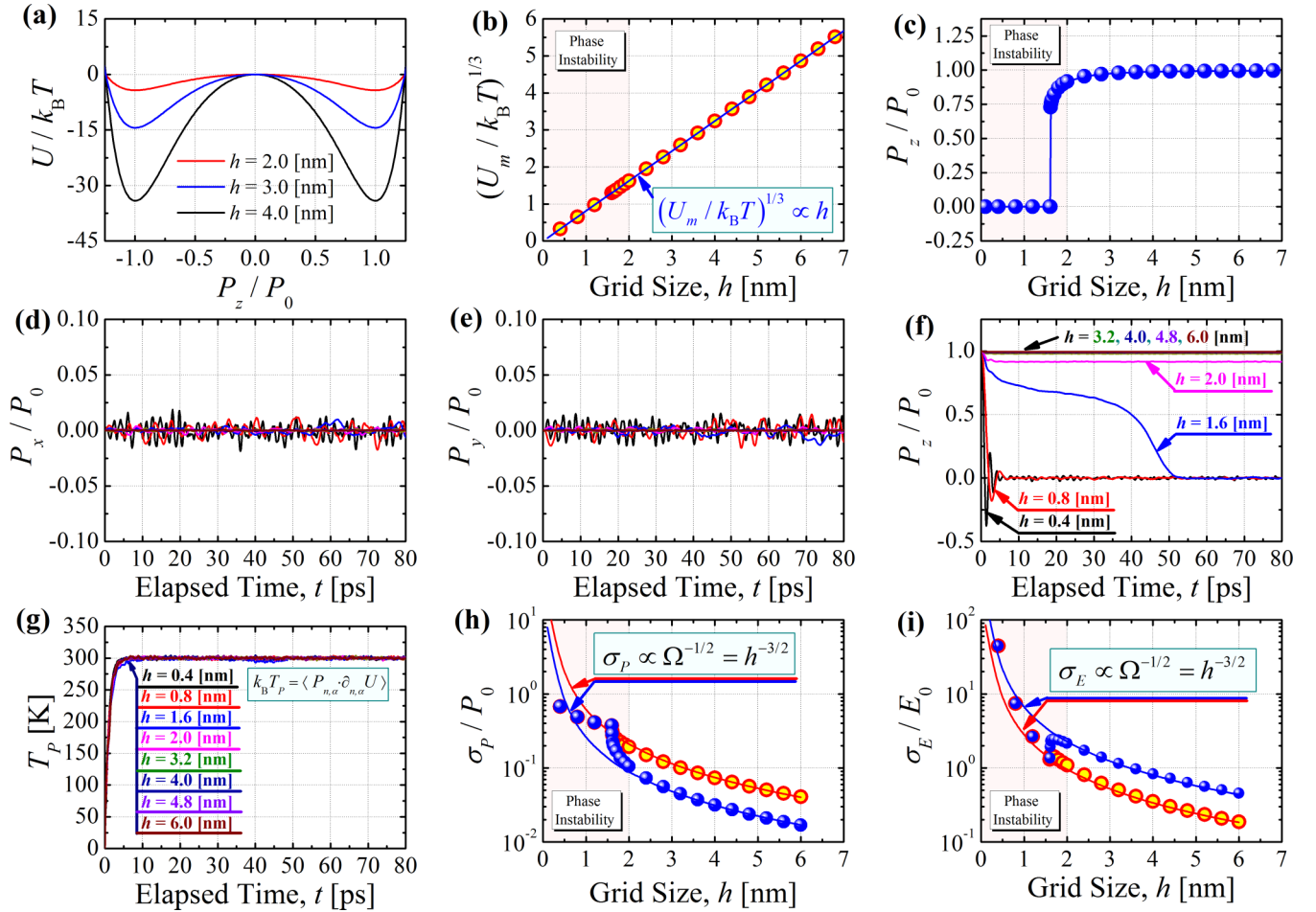


FIG. 4. (a) The potential landscape U along P_z for the cases of $h = 2.0, 3.0, 4.0$ nm. (b) The competition of $U_m/k_B T$ is linearly proportional to the grid volume as h^3 . (c) The phase instability revealed in the PFM simulations with system discretized into small grids as $h < 2.0$ nm. (d)–(f) The time-evolution behaviors of P_α with $\alpha = x, y, z$. (g) The observed polarization temperature T_P in terms of $k_B T_P = \langle P_{n,\alpha} \partial_{n,\alpha} U \rangle$ (see Appendix C). (h)–(i) The fluctuations of polarization σ_P/P_0 and effective electric field σ_E/E_0 , where σ_P and σ_E are estimated following Eq. (23), and $E_0 = 9.6501 \times 10^6 \text{ Jm}^{-1}\text{C}^{-1}$ is a normalized constant. In (h) and (i), the red open circles represent the quantities along nonpolar directions (i.e., x and y directions) and blue solid dots stand for data along the polar direction (i.e., z direction).

and thermodynamics, we have to pay more attentions on the rationality and reliability when promoting PFM scheme to study the atomic-scale polarization dynamical behavior. In atomic scale, the thermal fluctuations of polarization become more significant and play the important role on the evolution behaviors. In the following, we will perform the duplicate PFM simulations as those shown in Fig. 2 based on second TDGL equation of Eq. (5). For each simulation case, the box is set as $64h \times 64h \times 64h$, and the grid-meshing size h is set in the range from 0.4 to 6.8 nm.

Figure 4 shows the simulation results. Let us check the thermodynamic equivalent relation for first. Referring to Eq. (19), the strength of thermal fluctuation denoted by $k_B T_P$ can be characterized by the statistics of polarization dynamics, which is further equal to the stochastic actions of its Langevin heat bath denoted by $\kappa/2\gamma = k_B T_x$. For all the PFM simulation systems discretized into various grid sizes of h considered, the equivalent relation of the thermodynamic zeroth law is well confirmed in Fig. 4(g) in terms of $T_P = \langle P_{n,\alpha} \partial_{n,\alpha} U \rangle / k_B$, in accordance with conjugate variables theorem [39] (see details in Appendix C). However, the

time-evolution behaviors of $P_z(t)$ plotted in Fig. 4(f) reveal the unexpected phase instability when $h < 2$ nm.

For $P_{n,\alpha}$ staying at one of the minima of the potential fields demonstrated in Fig. 4(a), it would hop between two stable states with thermal assistance. According to Kramers' theory [51], the probability of $P_{n,z}$ escaping the potential well is determined by the competition $U_m/k_B T$ between the energy barrier U_m and the thermal energy $k_B T$. Note that the value of $U_m/k_B T$ is linearly proportional to $\Omega = h^3$ as $(U_m/k_B T)^{1/3} \propto h$ [see in Fig. 4(b)]. Therefore, for the systems discretized into large grids, $U_m/k_B T$ is sufficiently large to significantly avoid the possible transition of $P_{n,z}$ between its two stable states. For example, plotted in Fig. 4(b), $U_m/k_B T > 10$ when $h > 2$ nm, giving rise to the polar state of $P_z \approx P_0$ as expected [see in Fig. 4(c)]. In contrast, for the systems discretized into small grids, e.g., $h < 2.0$ nm, the value of $U_m/k_B T$ reduces rapidly [see in Fig. 4(b)], so that the system could not stay at $P_z = P_0$, and it will hop between $\pm P_0$. Therefore, for the long-term behavior, the probability for the system staying at P_0 is almost equal to that at $-P_0$, giving rise to the phase instability as $P_z = 0$ [see the shaded region in Fig. 4(c)]. On the other

hand, the conjecture can be made that the phase transition temperature decreases as the reduction of the discretized grid size in PFM simulations. For instance, BTO should stay at T phase at 300 K, but it reveals a C-phase structure in the case of $h < 2.0$ nm. This conjecture is well confirmed by the results of the fluctuations of polarization σ_P and electric field σ_E shown in Figs. 4(h) and 4(i), respectively, which are defined according to the fluctuation theorem [52] as

$$\begin{cases} \sigma_{P,\alpha}^2 = \langle P_{n,\alpha}^2 \rangle - \langle P_{n,\alpha} \rangle^2 = k_B T \chi_{\alpha\alpha} / \Omega, \\ \sigma_{E,\alpha}^2 = \langle E_{n,\alpha}^2 \rangle - \langle E_{n,\alpha} \rangle^2 = k_B T / (\chi_{\alpha\alpha} \Omega), \end{cases} \quad (23)$$

where $\chi_{\alpha\alpha}$ is the component of the susceptibility tensor χ . Figures 4(h) and 4(i) indicate the relations of $\sigma_P^2 \propto \Omega^{-1}$ and $\sigma_E^2 \propto \Omega^{-1}$ are well satisfied when $h > 2.0$ nm, which are apart from the prediction when $h < 2.0$ nm.

In addition, for the polarization dynamics system of Γ_1 governed by the first TDGL equation of Eq. (4), although there is no inertial term involved because it shares the same free-energy functional $F[\mathbf{P}]$ or potential field $U(\{P_i\})$ with that of Γ_2 governed by the second TDGL equation, similar phase instability is also found by performing the PFM simulations based on the first TDGL equation. Therefore, the inertial term introduced is not the key factor responsible for the phase instability when adopting the small discretized grids in the PFM simulations. Furthermore, we fix the numbers of meshing grids N in the simulations shown in Fig. 4, so that the total volume V of the interested system decreases with smaller grid size discretized, as $V = Nh^3$. Otherwise, when we fix V , N will then increase as decreasing the grid size h , as $N = V/h^3$. Because the periodic boundary condition is applied to the system of perfect BTO structure, the selection of a sufficient large V has little influence to the simulation results. It has been checked that the phase instability still occurs when $h < 2$ nm, if fixing V in PFM simulations.

In this regard, due to the small values of the competition $U_m/k_B T$ between the conservative potential and thermal energy, PFM simulations of polarization dynamics reveal the unexpected phase instability in the cases of small grid discretization. Note that the value of $U_m/k_B T$ depends on the grid size h set in the numerical approach of PFM simulations, that is because the potential force field U is size dependent since the free-energy density is the key quantity fitted in conventional PFM scheme, but the thermal fluctuation strength $k_B T$ is independent of grid size h after the discretization operation.

B. Viable solution

From the information revealed in the above PFM simulation results, it can be found that the random force provided by Langevin heat bath ensures the statistical nature of polarization dynamics, and the resulting thermal fluctuations indeed give rise to the non-negligible effects [24]. In principle, the simulation results in PFM should not rely on the meshing grid size h adopted in numerical approach. However, because the free-energy functional $F[\mathbf{P}]$ or potential field $U(\{P_i\})$ used in current PFM scheme was developed without accounting for the thermal fluctuations [20,44], the contradiction between the fluctuation induced by random force and the atomic-scale grid discretization exists naturally, both of which, unfortunately,

are the necessary conditions for the issues about studies of the atomic spatiotemporal polarization dynamical responses. Researchers [24] have been aware to find appropriate ways out of the dilemma owed to the presence of random force.

As mentioned above, the small values of $U_m/k_B T$ lead to the phase instability in the discretized system with $h < 2$ nm. Therefore, a simple but effective way to get rid of the contradiction between thermal fluctuation and small grid discretization is to enlarge the values of $U_m/k_B T$ by reconstructing the potential field $U(\{P_i\})$. For BTO, the potential field U developed in Refs. [44,45] has been proved to correctly reproduce the sequence of the phase transition. Based on this potential field, we just enlarge the values of $U_m/k_B T$ in a simple but appropriate way by multiplying the original U with a constant factor for all the temperatures considered, which ensures $U_m/k_B T$ to be large enough to avoid the phase instability for the system discretized with $h = 0.4$ nm.

Figure 5(a) plots the landscape of revised potential field in the case of $h = 0.4$ nm along the spontaneous polarization direction P_α corresponding to different phase at $T = 150$ K of rhombohedral (R) phase with P along $\langle 111 \rangle$ direction, 250 K of orthorhombic (O) phase with P along $\langle 011 \rangle$ direction, 300 K of T phase with P along $\langle 001 \rangle$ direction, and 400 K of cubic (C) phase of paraelectrics, respectively. After revision, the values of $U_m/k_B T > 10$ at various temperatures from 10 to 385 K (covering all the polar phases existing in BTO) are believed to be sufficiently large to avoid the phase instability, as demonstrated in Fig. 5(b). In this consideration, we perform the PFM simulations for the polarization dynamical system described by the Hamiltonian \mathcal{H}_2 for Γ_2 in Eq. (8), which is discretized into 64 cubic grids along each Cartesian dimension with grid size of $h = 0.4$ nm. The system is embedded in Langevin heat bath denoted by T ranging from 10 to 450 K, where the phase-space trajectories of polarization are obtained by solving the second TDGL equation of Eq. (5). Plotted in Fig. 5(c), for all temperatures considered here, both the observed kinetic temperature and configuration temperature, estimating the polarization temperature T_p following Eq. (19) (see in Appendix C), are well consistent with that of the Langevin heat bath T_x , which confirms the thermodynamic zeroth law for the polarization dynamics. This thermodynamic feature can be further confirmed by the probability distribution ρ of the conjugated momentum p in Fig. 5(e), which follows the Maxwell-Boltzmann distribution, as

$$\rho(p)dp = \frac{1}{\sqrt{2\pi k_B T}} \exp\left(-\frac{p^2}{2k_B T}\right) dp \quad (24)$$

with $p_{n,\alpha} = \sqrt{\mu} \dot{P}_{n,\alpha}$, so that

$$k_B T = \int_{-\infty}^{\infty} p^2 \rho(p) dp = \langle \mu \dot{P}_{n,\alpha}^2 \rangle. \quad (25)$$

Besides, the observed total polarization calculated by $P_\alpha = \langle P_{n,\alpha} \rangle$ is plotted in Fig. 5(d), where the sequence of phase transition in BTO is well reproduced as that in Ref. [44], with the transition temperatures are ~ 202 K between R-O phases, ~ 281 K between O-T phases, and ~ 395 K between T-C phases, respectively. In this regard, we can conclude that the value of $U_m/k_B T$ is indeed the key factor leading to the phase instability of the Langevin polarization dynamics

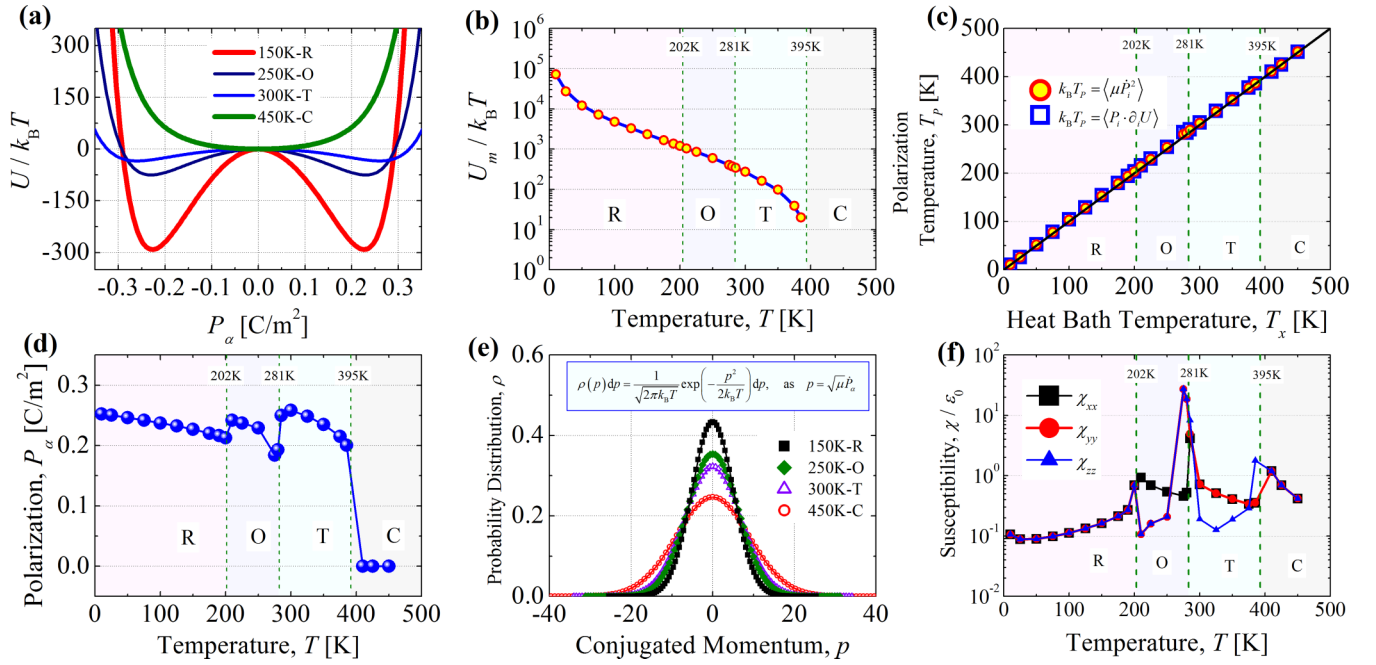


FIG. 5. (a) The revised potential landscape along the spontaneous polarization at various temperatures, i.e., 150 K of R phase, 250 K of O phase, 300 K of T phase, and 450 K of C phase. (b) The revised competition strength of $U_m/k_B T$ at various temperatures ranging from 10 to ~ 385 K. (c) The polarization temperatures estimated following Eq. (19) (see in Appendix C). (d) The observed polarization as $P_\alpha = \langle P_{n,\alpha} \rangle$, where the sequence of ferroelectric phase transition is correctly reproduced, with $T_C \sim 202$ K for R-O, ~ 281 K for O-T, and ~ 395 K for T-C phase transitions, respectively. (e) The probability distribution ρ of the conjugated momentum p at $T = 150, 250, 300,$ and 400 K, which follows the Maxwell-Boltzmann distribution. (f) The temperature dependence of the calculated susceptibility $\chi_{\alpha\alpha}$.

of PFM simulations in ferroelectrics. However, the simple revision by enlarging the values of $U_m/k_B T$ is to compress the effects of thermal fluctuations equivalently. Therefore, the resulting susceptibility $\chi_{\alpha\alpha}$ calculated following fluctuation theorem of Eq. (23) is rather underestimated, although whose temperature dependence is consistent with the predictions of classical molecular dynamics reported [15].

Further, this underestimation of thermal fluctuations under the revised potential force field has significant influence to the dynamical behaviors of polarization, in particular, when the ferroelectric system experiences a nonequilibrium process under the applied external field. Plotted in Fig. 6, we repeat the polarization reversal switching process from P_A to P_B

illustrated in Fig. 1, which is similar to that shown in Fig. 3. Here, we only present the simulation results based on the stochastic second TDGL equation, i.e., Eq. (5) or case II in Eq. (21). Due to the compression of thermal fluctuations, the time-evolution behavior of total polarization P_z in Fig. 6(a) acts like an overdamped oscillation, compared to that in Fig. 3(a). In addition, the reversal external field applied $E_{\text{ext}} = -2.5 \times 10^9$ V/m is required to make a substantial polarization switching, which is far larger than $E_{\text{ext}} = -1.41 \times 10^7$ V/m before the revision. Although the thermal effects of polarization dynamics are underestimated, the stochastic feature of polarization switching can be still well reproduced because of the presence of random force, for

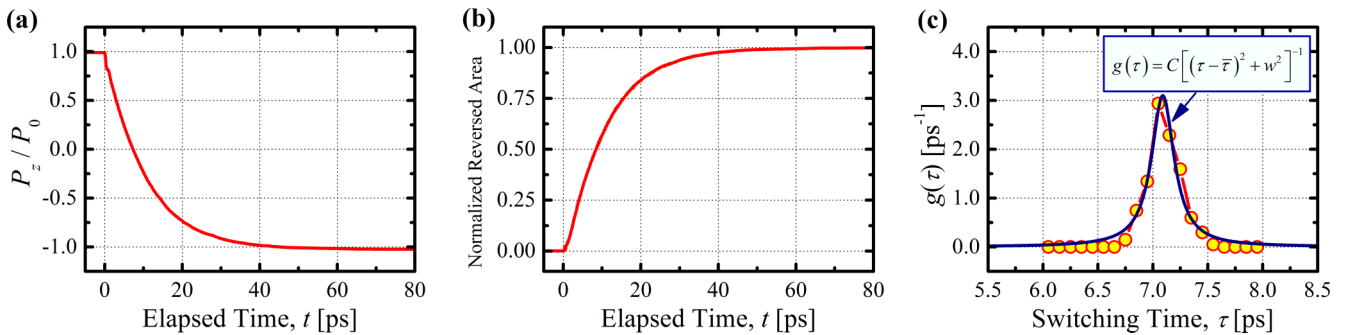


FIG. 6. The simulation results of polarization reversal switching process under an applied electric field $E_{\text{ext}} = -2.5 \times 10^9$ V/m, similar to that shown in Fig. 3, but only the simulation based on stochastic TDGL equation [i.e., case II in Eq. (21) or Eq. (5)], with the revised potential field U shown in Fig. 5(a) adopted. (a) The time evolution of total polarization; (b) the time-dependent normalized reversed area; (c) the statistics of switching time τ induced by thermal fluctuations arising from the random force, which also well satisfy the Lorentzian distribution shown in Eq. (22).

example, the gradual increase of normalized reversal area and the Lorentzian distribution of the estimated switching time τ from 200 repeated simulations, respectively, plotted in Figs. 3(b) and 3(c).

C. Further discussion

The contradiction of thermal fluctuation induced by random force and the phase instability in case of small grid discretization adopted in PFM simulations is naturally a result of thermodynamics and microdynamics. This contradiction is originated from the incompatibility between the free-energy functional or potential force field and random force used in TDGL equations. From the analysis presented in this paper, a viable solution to get out of this dilemma is to reconstruct the potential force field and enlarge the values of $U_m/k_B T$, which requires further investigation starting from the first-principles studies on the fundamental interactions inside the ferroelectric system. Otherwise, we can retain the random force maintaining the thermodynamics, but not to discretize the system into atomic-scale grids, so to avoid the possible phase instability. Referring to the atomistic modeling scheme (e.g., effective Hamiltonian method for polarization dynamics), the potential force field exerted by the dynamical DOF in a many-body system has a different physical essence from the free energy. In principle, a potential force field describes the many-body inter-DOF interaction, but the free energy is a specific-process-related thermodynamic quantity. Therefore, to reconstruct the potential force field for polarization dynamics that is compatible with the thermal fluctuations at finite temperature, aside from the onsite potential field, there should be interactive terms between different grid polarizations in PFM simulation scheme, like dipole-dipole interaction. In this regard, appropriately carrying out the thermal fluctuations in current PFM scheme is a key step toward the multiscale modeling on polarization dynamics, i.e., bridging the microdynamics and thermodynamics. With correctly reproducing the thermal fluctuations of polarization system, the second-order response coefficients, like the susceptibility, pyroelectric coefficient, piezoelectric coefficient, or other constitutive response coefficients, can be directly estimated based on the dynamical responses polarization under the corresponding external stimulations, following the similar approach adopted in atomistic simulations [53].

In addition, to well predict the polarization dynamical responses, we have to pay attention to other dynamical parameters in the TDGL equation, like μ and γ in Eq. (5). As the conservative potential profile $U(P)$ links to how easily the phase transition of polarization dynamics occurs under the external environment, μ and γ characterize how fast the phase transition occurs. In thermodynamics, any arbitrary phase transition process is to minimize the total free energy of the system interested, during which the conservative potential relaxes accompanied with the heat dissipation. Accordingly, μ relates to the potential and kinetic energetic exchange, and γ denotes the heat dissipation. Therefore, the transition rate is determined by the characteristic thermal vibration frequencies in a conservative-potential-controlled quasiequilibrium process, and the heat-dissipation rate in a heat-dissipation-controlled nonequilibrium process.

This is a universal thermodynamic phenomenon occurring in various cases, like solute diffusion in crystal [54] and magnetic skyrmion transport [55]. For example, for the polarization transition process governed by the second TDGL equation, the effective mass μ is in principle a second-rank tensor, whose component $\mu_{\alpha\alpha}$ is associated with the characteristic vibrational frequency ω_α of the polarization P_α , as

$$\mu_{\alpha\alpha} = \frac{1}{\omega_\alpha^2} \frac{\partial^2 U}{\partial P_\alpha^2}. \quad (26)$$

Referring to Eqs. (C5) and (C6), we can get

$$\frac{\mu_{\alpha\alpha}}{\Omega} = \frac{1}{\chi_{\alpha\alpha} \omega_\alpha^2}. \quad (27)$$

Therefore, μ mainly reflects the fluctuation characteristics when the system under equilibrium states, and it also determines the transition rate when the ferroelectric system experiences a conservative-potential-controlled quasiequilibrium phase transition process with $U_m \gg k_B T$ [15]. For example, $\mu/\Omega = 5 \times 10^{-11} \text{ Jm}^4 \text{ C}^{-2} \text{ s}^2$ is used in this paper, which is fitted on the basis of the experimental measurement of domain-wall motion reported in Refs. [22,23] with the characteristic frequency as $\omega_\alpha \sim 10^9$ Hz. The value of μ/Ω is ~ 6 orders of magnitude larger than that reported in Ref. [56]. It makes sense in accordance with the definition in Eq. (27) because the value of μ/Ω in the latter case is fitted from the characteristic vibrational frequencies of phonon modes ($\omega_\alpha \sim 10^{12}$ Hz) related to the collective vibrations of the unit-cell electric dipoles. On the other hand, γ characterizes the dissipation nature of polarization phase transition, and determines the transition rate of a heat-dissipation-controlled nonequilibrium process with $U_m \ll k_B T$ [15]. It is also associated with the so-called lifetime of phonon modes related to the polarization dynamics [15], which is equivalent to the phonon widths [56].

To sum up, because polarization dynamics is a multiscale dynamical process, the ultimate solution is to build up a practical multiscale modeling scheme following the coarse-grained approach, where the dynamical responses of the multi-ingredients responsible for the observed polarization can be described in a unique simulation framework. As addressed in Ref. [15], the generalized Langevin equation, e.g., the second TDGL equation, could be one of the possible candidates, which can naturally and intrinsically satisfy the principles of many-body dynamics and statistical thermodynamics in a unique theoretical framework. In fact, to build up such a scheme, it has to make a clear mechanistic understanding on the physical picture of the related quantities determining the polarization dynamics, i.e., (1) the conservative potential to obtain the information of what stable states does the macroscopic polarization observed evolve, and (2) the effective mass and dissipative parameter to characterize the temporal behaviors of polarization evolution. In this case, several challenges should be taken over with further investigation, for example: (1) How to characterize and describe physical processes of polarization dynamics at various spatiotemporal scales? (2) How to apply the coarse-grained operation to polarization dynamics from atomic scale to the larger scales, and ensure consistency in microdynamics

and thermodynamics, as well as the parameter transfer among different scales [57]? (3) How to describe the coupling mechanisms of polarization dynamics $\{P_i\}$ and other DOF $\{x_j\}$ mentioned in Eq. (6), and to coarse grain the dynamical actions of $\{x_j\}$ as the thermodynamic environment to the dynamics of $\{P_i\}$? Aside from the dynamical equation, the PFM scheme of polarization dynamics is developed on the phenomenological thermodynamic theory, where the big challenge is how to clarify the interaction between spontaneous (or critical) polarization and nonspontaneous (noncritical) polarization. Current thermodynamic formula of the free-energy functional supposes that effects of nonspontaneous polarization can be described by the background dielectric constant [58,59]. However, recent studies suggest that it is not a material-independent constant, which has been shown to spoil the self-consistency of the Landau theory [60]. In our opinion, discussion about the fundamental physics for polarization dynamics is in its infancy, and further investigation is required for deep insight.

IV. CONCLUSION

In this paper, we discussed the underlying physical picture of phase field model (PFM) scheme of polarization dynamics on the basis of the stochastic time-dependent Ginzburg-Landau (TDGL) equation (equivalent to the Langevin equation). Applying the operation of numerical discretization to solve the nonlinear variational TDGL equation maps the original three-dimensional continuous polarization dynamics to be a many-body stochastic one. The random force naturally appears in the Langevin equation of polarization dynamics as the fluctuation actions arising from its Langevin heat bath. Together with the dissipation actions, the random force guarantees the correctness of thermodynamics. In addition, the participation of random force can result in a different mechanism of heat dissipation in the process of polarization dynamical responses under external field. However, the thermal fluctuations induced by the random force would result in the phase instability with small discretized grids applied in simulations based on currently used PFM scheme. Performing PFM simulations of BaTiO₃ (BTO) at 300 K as examples, it is found that the energy barrier is not large enough to counteract the thermal fluctuation, leading to the unexpected phase instability. This contradiction between random force and free-energy functional used in TDGL equations of current PFM simulation scheme is a natural result of thermodynamics and microdynamics. In our opinion, the viable solution is to reconstruct the potential force field. Adopting a simple way to enlarge the corresponding energy barrier, the phase instability is examined to be eliminated and the ferroelectric phase transition in BTO can be then correctly reproduced. Meanwhile, the thermodynamic zeroth law in polarization dynamics is also well satisfied. However, this simple way results in the underestimation of the thermal fluctuation. In this regard, promoting the PFM scheme to the atomic-scale polarization dynamics, one should carefully check the rationality and reliability in the statistical thermodynamic point of view. In particular, the atomic-scale thermal fluctuations for the polarization element discretized in PFM simulations at finite temperatures will play an important role on the evolution

behaviors of polarization. Furthermore, we also address our opinion on the future development of the multiscale modeling scheme for polarization dynamics. We hope our discussion of the underlying physics could provide useful ideas for the development of the multiscale modeling scheme for polarization dynamics in ferroelectrics based on phase field models.

ACKNOWLEDGMENTS

We thank our colleagues in Sun Yat-sen University, including W. Zhu, X. Luo, L. Li, L. Zhu, and K. Lai, for helpful discussion and valuable comments on the manuscript. This work was supported by the National Natural Science Foundation of China (NSFC) (Grants No. 11804286, No. 12172396, No. 12132020, No. 12072379, No. 12002400, No. 11904415, and No. 11972382), the National Natural Science Foundation of Guangdong Province, China (Grants No. 2021A1515010346, No. 2021A1515010348, and No. 2021B1515050021), and the Guangdong Basic and Applied Basic Research Foundation (Grant No. 2022A1515010249). The simulations reported were performed on resources provided by the National Supercomputer Center in Guangzhou, the Guangdong Provincial Key Laboratory of Magnetoelectric Physics and Devices (LaMPad) and the Centre for Physical Mechanics and Biophysics (CPMB) in School of Physics in Sun Yat-sen University.

H.W. and J.L. contributed equally to this paper.

APPENDIX A: PFM SIMULATION DETAILS

In the conventional PFM scheme for polarization dynamics, the free-energy functional $F[\mathbf{P}]$ for a continuous three-dimensional polarization field $\mathbf{P}(\mathbf{r})$ is defined as

$$F[\mathbf{P}] = \int_V f(\mathbf{P}, \nabla\mathbf{P}, \mathbf{r}) dV, \quad (\text{A1})$$

where f is the free-energy density. For a bulk ferroelectric system without the surface effects, f is usually written as

$$f = f_{\text{Land}}(\mathbf{P}) + f_{\text{grad}}(\nabla\mathbf{P}) + f_{\text{elec}}(\mathbf{P}) + f_{\text{elas}}(\mathbf{P}). \quad (\text{A2})$$

Here, $f_{\text{Land}}(\mathbf{P})$ is the Landau bulk free-energy density expressed in terms of the Taylor expansion of P_α (P_α is the α component of \mathbf{P} along the Cartesian dimension, where $\alpha, \beta = x, y, z$) [44,45],

$$\begin{aligned} f_{\text{Land}} = & a_1 \sum_{\alpha} P_{\alpha}^2 + a_{11} \sum_{\alpha} P_{\alpha}^4 + a_{12} \sum_{\alpha>\beta} P_{\alpha}^2 P_{\beta}^2 \\ & + a_{111} \sum_{\alpha} P_{\alpha}^6 + a_{112} \sum_{\alpha\neq\beta} P_{\alpha}^4 P_{\beta}^2 \\ & + a_{123} \prod_{\alpha} P_{\alpha}^2 + a_{1111} \sum_{\alpha} P_{\alpha}^8 \\ & + a_{1112} \sum_{\alpha\neq\beta} P_{\alpha}^6 P_{\beta}^2 + a_{1122} \sum_{\alpha>\beta} P_{\alpha}^4 P_{\beta}^4 \\ & + a_{1123} \sum_{\alpha} P_{\alpha}^2 \prod_{\beta} P_{\beta}^2. \end{aligned} \quad (\text{A3})$$

All the a are the expansion parameters, whose values are listed in Table I, and also can be referred to Refs. [44,45]. $f_{\text{grad}}(\nabla\mathbf{P})$

TABLE I. Parameters used in PFM simulations of current work for BaTiO₃, which can be referred to Refs. [44,45].

Parameter	Value
a_1	$(T - 388) \times 4.124 \times 10^5 \text{ JmC}^{-2}$
a_{11}	$-2.097 \times 10^8 \text{ Jm}^5\text{C}^{-4}$
a_{12}	$7.974 \times 10^8 \text{ Jm}^5\text{C}^{-4}$
a_{111}	$1.294 \times 10^9 \text{ Jm}^9\text{C}^{-6}$
a_{112}	$-1.950 \times 10^9 \text{ Jm}^9\text{C}^{-6}$
a_{123}	$-2.500 \times 10^9 \text{ Jm}^9\text{C}^{-6}$
a_{1111}	$3.863 \times 10^{10} \text{ Jm}^{13}\text{C}^{-8}$
a_{1112}	$2.529 \times 10^{10} \text{ Jm}^{13}\text{C}^{-8}$
a_{1122}	$1.637 \times 10^{10} \text{ Jm}^{13}\text{C}^{-8}$
a_{1123}	$1.367 \times 10^{10} \text{ Jm}^{13}\text{C}^{-8}$
G_1	$4.4539 \times 10^{-11} \text{ Jm}^3\text{C}^{-2}$
G_2	$2.2270 \times 10^{-11} \text{ Jm}^3\text{C}^{-2}$
ϵ_b	$4.4271 \times 10^{-11} \text{ J}^{-1}\text{m}^{-1}\text{C}^2$
C_{11}	$19.8 \times 10^{10} \text{ Jm}^{-3}$
C_{12}	$9.60 \times 10^{10} \text{ Jm}^{-3}$
C_{44}	$12.2 \times 10^{10} \text{ Jm}^{-3}$
Q_{11}	$1.104 \times 10^{-1} \text{ m}^4\text{C}^{-2}$
Q_{12}	$-4.520 \times 10^{-2} \text{ m}^4\text{C}^{-2}$
Q_{44}	$2.950 \times 10^{-2} \text{ m}^4\text{C}^{-2}$
γ for Γ_1	$2 \times 10^1 \text{ J}^{-1}\text{m}^{-4}\text{C}^2\text{s}^{-1}$
γ for Γ_2	$h^3 \times 5 \times 10^{-2} \text{ Jm}^4\text{C}^{-2}\text{s}$
μ	$h^3 \times 5 \times 10^{-11} \text{ Jm}^4\text{C}^{-2}\text{s}^2$

in Eq. (A2) is the gradient term as

$$f_{\text{grad}} = \sum_{\alpha,\beta} \frac{G_l}{2} \left(\frac{\partial P_{n,\alpha}}{\partial r_\beta} \right)^2, \quad (\text{A4})$$

where $G_l = G_1$ if $\alpha = \beta$ and $G_l = G_2$ if $\alpha \neq \beta$, with G_1 and G_2 being the gradient coefficients, whose values are listed in Table I. $f_{\text{elec}}(\mathbf{P})$ in Eq. (A2) is the electrostatic term as

$$f_{\text{elec}}(\mathbf{P}) = -\mathbf{P} \cdot \mathbf{E} - \frac{1}{2} \epsilon_b \mathbf{E}^2, \quad (\text{A5})$$

where \mathbf{E} is the total electrostatic field, including the external electric field \mathbf{E}_{ext} and depolarization field \mathbf{E}_d , as $\mathbf{E} = \mathbf{E}_{\text{ext}} + \mathbf{E}_d$; ϵ_b is the background dielectric permittivity. $f_{\text{elas}}(\mathbf{P})$ in Eq. (A2) is the electrostrictive term as

$$f_{\text{elas}}(\mathbf{P}) = \sum_{\alpha\beta\lambda\nu} \frac{1}{2} C_{\alpha\beta\lambda\nu} (e_{\alpha\beta} - e_{\alpha\beta}^0) (e_{\lambda\nu} - e_{\lambda\nu}^0), \quad (\text{A6})$$

where $C_{\alpha\beta\lambda\nu}$ are elastic stiffness coefficients, $e_{\alpha\beta}$ are eigenstrain components of the strain tensor \mathbf{e} , and $e_{\alpha\beta}^0$ is the eigenstrain induced by the electromechanical coupling, depending on the spontaneous polarization as $e_{\alpha\beta}^0 = \sum_{\lambda\nu} Q_{\alpha\beta\lambda\nu} P_\lambda P_\nu$ with $Q_{\alpha\beta\lambda\nu}$ being the electrostrictive coefficients. The values of $C_{\alpha\beta\lambda\nu}$ and $Q_{\alpha\beta\lambda\nu}$ are listed in Table I.

APPENDIX B: FROM VARIATIONAL EQUATION TO DIFFERENTIAL ONE FOR POLARIZATION DYNAMICS

For the simplest case of a ferroelectric system considered in this work, which contains the monodomain, and no external stress and electric field applied, the free-energy functional can

be simplified as the form of

$$F[\mathbf{P}] = \int_V (f_{\text{self}}(\mathbf{P}) + f_{\text{grad}}(\nabla\mathbf{P})) dV, \quad (\text{B1})$$

where $f_{\text{self}}(\mathbf{P}) = f_{\text{Land}}(\mathbf{P}) + f_{\text{elec}}(\mathbf{P}) + f_{\text{elas}}(\mathbf{P})$ is the function of the polarization vector \mathbf{P} at a specific location, and the gradient term depends on polarization vectors of different locations as written by Eq. (A4). In this consideration, these two terms are, respectively, named as the local and nonlocal potentials in literature.

After meshing the continuous system into grids, the continuous variational TDGL equations of Eqs. (1) and (3) can be thus transferred as the discretized ones as

$$\begin{cases} \dot{P}_{n,\alpha} = -L \frac{\delta F}{\delta P_{n,\alpha}} + \xi_{n,\alpha}(t), \\ \mu' \ddot{P}_{n,\alpha} + \gamma' \dot{P}_{n,\alpha} + \delta_{n,\alpha} F = \xi'_{n,\alpha}(t), \end{cases} \quad (\text{B2})$$

where $F = F(\{P_{n,\alpha}\})$ is the many-body free-energy function corresponding to the free-energy functional $F[\mathbf{P}]$, with $n = 1, 2, \dots, N$ and $\alpha = x, y, z, i.e.,$

$$F[\mathbf{P}] \mapsto F(\{P_{n,\alpha}\}) = \Omega \sum_{n,\alpha} f(\{P_{n,\alpha}\}), \quad (\text{B3})$$

where $f = f_{\text{self}} + f_{\text{grad}}$. Note that $\delta F / \delta P_{n,\alpha}$ is a functional derivative of the simplest functional with fixed boundary. According to Euler-Lagrange variation theorem, the effective electric field $E_{n,\alpha}$ governing the dynamics of grid polarization of $P_{n,\alpha}$ in Eqs. (4) and (5) can be derived as

$$\begin{aligned} E_{n,\alpha} &= -\frac{\delta F}{\delta P_{n,\alpha}} = -\frac{\partial f_{\text{self}}}{\partial P_{n,\alpha}} + \sum_{\beta} \frac{\partial}{\partial r_\beta} \left(\frac{\partial f_{\text{grad}}}{\partial w_{\alpha,\beta}^n} \right) \\ &\equiv E_{n,\alpha}^{\text{self}} + E_{n,\alpha}^{\text{grad}}, \end{aligned} \quad (\text{B4})$$

where we define $E_{n,\alpha}^{\text{self}}$ and $E_{n,\alpha}^{\text{grad}}$ as the effective electric field governing the polarization of $P_{n,\alpha}$, respectively, arising from the terms related to f_{self} and f_{grad} . Considering the form of f_{grad} written in Eq. (A4), we have

$$E_{n,\alpha}^{\text{grad}} = \sum_{\beta} G_l \frac{\partial w_{\alpha,\beta}^n}{\partial r_\beta}, \quad \text{as } w_{\alpha,\beta}^n = \frac{\partial P_{n,\alpha}}{\partial r_\beta}. \quad (\text{B5})$$

Because

$$\left(\frac{\partial w_{\alpha,\beta}^n}{\partial P_{n,\alpha}} \right) \left(\frac{\partial P_{n,\alpha}}{\partial r_\beta} \right) \left(\frac{\partial r_\beta}{\partial w_{\alpha,\beta}^n} \right) = -1, \quad (\text{B6})$$

then

$$\frac{\partial w_{\alpha,\beta}^n}{\partial r_\beta} = -\frac{\partial P_{n,\alpha}}{\partial r_\beta} \frac{\partial w_{\alpha,\beta}^n}{\partial P_{n,\alpha}} = -\frac{1}{2} \frac{\partial}{\partial P_{n,\alpha}} \left(\frac{\partial P_{n,\alpha}}{\partial r_\beta} \right)^2 \quad (\text{B7})$$

so we can get

$$E_{n,\alpha}^{\text{grad}} = -\frac{\partial}{\partial P_{n,\alpha}} \sum_{\beta} \frac{G_l}{2} \left(\frac{\partial P_{n,\alpha}}{\partial r_\beta} \right)^2. \quad (\text{B8})$$

Combining Eqs. (B3), (B4), (B5), and (B8), we can get

$$E_{n,\alpha} = -\frac{\delta F}{\delta P_{n,\alpha}} = -\frac{\partial f}{\partial P_{n,\alpha}} = -\frac{1}{\Omega} \frac{\partial F}{\partial P_{n,\alpha}}. \quad (\text{B9})$$

Therefore, the discretized variational TDGL of Eq. (B2) can be rewritten as

$$\begin{cases} \dot{P}_{n,\alpha} = -\frac{L}{\Omega} \frac{\partial F}{\partial P_{n,\alpha}} + \xi_{n,\alpha}(t), \\ \mu' \ddot{P}_{n,\alpha} + \gamma' \dot{P}_{n,\alpha} + \frac{1}{\Omega} \frac{\partial F}{\partial P_{n,\alpha}} = \xi'_{n,\alpha}(t). \end{cases} \quad (\text{B10})$$

In this regard, the free energy $F(\{P_{n,\alpha}\})$ in Eq. (B3) acts like a conserved potential force field for $\{P_{n,\alpha}\}$. If defining $U(\{P_{n,\alpha}\}) = F(\{P_{n,\alpha}\})$, $\gamma = L/\Omega$ in the first TDGL equation, and $\mu = \mu'\Omega$, $\gamma = \gamma'\Omega$, and $\xi_{n,\alpha} = \xi'_{n,\alpha}\Omega$ in the second TDGL equation, we can achieve the classical Langevin equations illustrated as Eqs. (4) and (5) in the main context for polarization dynamics, that

$$\begin{cases} \dot{P}_i = -\gamma \partial_i U + \xi_i(t), \\ \mu \ddot{P}_i + \gamma \dot{P}_i + \partial_i U = \xi_i(t), \end{cases} \quad (\text{B11})$$

where i represents the degree of freedom (n, α), and $i = 1, 2, \dots, 3N$, so that P_i stands for $P_{n,\alpha}$.

In a word, starting from the free-energy functional and corresponding continuous variational TDGL equation, we derive the discretized differential TDGL equation and the corresponding potential force field, and the similar form can be obtained for a more general and complicated f_{grad} used in PFM simulations, like Eq. (2) in Ref. [32]. Further, f_{grad} might not be a conservative potential field, however, our numerical simulation results indicate that it does not affect the underlying physics in PFM simulations of polarization dynamics concerned in this work.

It should be noted that the above deduction is to incorporate the TDGL equation to the generalized Langevin equation of Eq. (9). In fact, in our PFM simulations, the TDGL equations are solved following the conventional numerical approaches described in the main context or reported in Refs. [45,50], as well as other associated literature cited in Ref. [20].

APPENDIX C: POLARIZATION TEMPERATURE

For a microdynamic system, the thermodynamic temperature can be generally given according to the so-called hypervirial [35], which is familiar to the researchers engaged in molecular simulation:

$$\left\langle A \frac{\partial \mathcal{H}}{\partial X_i} \right\rangle = k_B T \left\langle \frac{\partial A}{\partial X_i} \right\rangle. \quad (\text{C1})$$

Here, X_i is the i th microdynamic degrees of freedom (DOF), \mathcal{H} is the Hamiltonian, and A could be any functions of X_i or other DOF involved in \mathcal{H} .

(1) For the ferroelectric system of Γ_2 with \mathcal{H}_2 of Eq. (8), with choice of $X_i = \mu \dot{P}_i$ and $A = \mu \dot{P}_i$, we can get the so-called kinetic temperature as

$$k_B T = \langle \mu \dot{P}_i^2 \rangle. \quad (\text{C2})$$

(2) For both systems of Γ_1 and Γ_2 , with the choice of $X_i = P_i$ and $A = P_i$, we can have the configurational temperature of

polarization dynamics,

$$k_B T = \left\langle P_i \frac{\partial \mathcal{H}}{\partial P_i} \right\rangle = \langle P_i \partial_i U \rangle, \quad (\text{C3})$$

where $\partial \mathcal{H} / \partial P_i = \partial U / \partial P_i = \partial_i U$.

(3) For both systems of Γ_1 and Γ_2 , choosing $X_i = P_i$ and $A = \partial \mathcal{H} / \partial P_i$, so that

$$k_B T = \frac{\langle |\partial_i \mathcal{H}|^2 \rangle}{\langle \partial_i^2 \mathcal{H} \rangle} = \frac{\langle |\partial_i U|^2 \rangle}{\langle \partial_i^2 U \rangle} \quad (\text{C4})$$

which is consistent with the conclusion derived from the Fokker-Planck equation.

Further, Eq. (C4) has another practical form based on fluctuation theorem. At thermal equilibrium states, the potential U can be expanded harmonically as

$$U = U_0 + \Omega \sum_{n,\alpha} \frac{(P_{n,\alpha} - P_\alpha)^2}{2\chi_{\alpha\alpha}}, \quad (\text{C5})$$

where U_0 is the static energy at $P_{n,\alpha} = P_\alpha$, and $\chi_{\alpha\alpha}$ is the component of the susceptibility tensor χ , so that

$$\langle \partial_{n,\alpha} U \rangle = 0 \quad \text{and} \quad \langle \partial_{n,\alpha}^2 U \rangle = \Omega \chi_{\alpha\alpha}^{-1}. \quad (\text{C6})$$

Defining the effective electric field $E_{n,\alpha}$ acting on $P_{n,\alpha}$ as $E_{n,\alpha} = -\Omega^{-1} \partial_{n,\alpha} U$, we can get

$$\begin{cases} E_\alpha \equiv \langle E_{n,\alpha} \rangle = 0, \\ \sigma_{E,\alpha}^2 \equiv \langle E_{n,\alpha}^2 \rangle - E_\alpha^2 = \Omega^{-2} \langle |\partial_{n,\alpha} U|^2 \rangle. \end{cases} \quad (\text{C7})$$

Referring to the definition of polarization temperature in Eq. (17), we can have

$$k_B T = \frac{\langle |\partial_{n,\alpha} U|^2 \rangle}{\langle \partial_{n,\alpha}^2 U \rangle} = \frac{\Omega^2 \sigma_{E,\alpha}^2}{\Omega \chi_{\alpha\alpha}^{-1}} = \Omega \chi_{\alpha\alpha} \sigma_{E,\alpha}^2, \quad (\text{C8})$$

which is consistent with the fluctuation theorem [52]. The polarization fluctuations under equilibrium could be also rewritten as [52]

$$\sigma_{P,\alpha}^2 = \langle P_{n,\alpha}^2 \rangle - P_\alpha^2 = \Omega^{-1} k_B T \chi_{\alpha\alpha} \quad (\text{C9})$$

so that

$$k_B T = \Omega \chi_{\alpha\alpha}^{-1} \sigma_{P,\alpha}^2. \quad (\text{C10})$$

Combining Eqs. (C8) and (C10), we can get the following relation as

$$k_B T = \Omega \sigma_{P,\alpha} \sigma_{E,\alpha}. \quad (\text{C11})$$

APPENDIX D: MATHEMATICAL EXPECTATION AND VARIANCE OF POLARIZATION DYNAMICS IN PFM SCHEME

According to statistical thermodynamics, it requires at least the mathematical expectation $\langle A \rangle$ and variance $\langle A^2 \rangle$ of any arbitrary thermodynamic quantity A , if we want to achieve the knowledge of a phase-space probability distribution function ϱ , based on which we have the chance to get the complete information of the dynamics and thermodynamics at equilibrium state. Take the polarization relaxation process from P_e to P_A illustrated in Fig. 1 as an example. The mathematical expectation $P(t) = \langle P_i(t) \rangle$ corresponds to

the dynamical behavior, and the variance $\sigma_P^2(t) = \langle P_i^2(t) \rangle - \langle P_i(t) \rangle^2$ is associated with the thermodynamics because $\sigma_P^2 \propto k_B T_P$ according to the fluctuation theorem. In other words, the variance σ_P^2 implies the thermodynamic zeroth law of the polarization dynamical system. For PFM simulations using TDGL equation to govern the polarization dynamics, as long as we get an appropriate free energy or conservative potential profile, the equilibrium state mathematical expectation of polarization dynamics $P(t)$ can be well reproduced, whether there is random force involved or not. This has been demonstrated by bunches of related studies in literature (see examples in the review paper of Ref. [20]). However, without the random force, there is no so-called thermal fluctuation as $\sigma_P^2(t) = 0$, when the system reaches the equilibrium states with $t \rightarrow \infty$. In the following, we will give the detailed analysis.

Given the conservative potential U based on the LGD theory of ferroelectrics, there are four TDGL equations we have discussed in the main context:

$$\left\{ \begin{array}{ll} \dot{P}_i + \gamma \partial_i U = 0, & \text{i.e., TDGL-A} \\ \dot{P}_i + \gamma \partial_i U = \xi_i(t), & \text{i.e., TDGL-B} \\ \mu \ddot{P}_i + \gamma \dot{P}_i + \partial_i U = 0, & \text{i.e., TDGL-C} \\ \mu \ddot{P}_i + \gamma \dot{P}_i + \partial_i U = \xi_i(t), & \text{i.e., TDGL-D.} \end{array} \right. \quad (\text{D1})$$

It has to be noted that each TDGL equation corresponds to a specific microdynamic system of polarization dynamics because each phase-space trajectory $\{P_i(t)\}$ and the probability distribution function $\varrho(\{P_i(t)\})$ are the synergistic results of actions of all the terms involved in the corresponding dynamical equation. In principle, these actions cannot simply accumulate.

For TDGL-A and TDGL-C, because there is no random force ξ involved, the phase-space trajectories of $\{P_i(t)\}$ are deterministic. During the process the system relaxes to $P_A = P_0$ from P_e near P_0 as illustrated in Fig. 1 (we denote $\Delta = P_e - P_0$, and assume $\Delta/P_0 \ll 1$). The phase trajectories governed by TDGL-A and TDGL-C can be, respectively, written as

$$\left\{ \begin{array}{l} P_i(t) = P_0 + \Delta e^{-t/2\tau}, \\ P_i(t) = P_0 + \Delta e^{-t/2\tau} \cos(\omega t), \end{array} \right. \quad (\text{D2})$$

where τ is the relaxation time, that $\tau = \chi/(2\gamma\Omega)$ for TDGL-A (see detail in Sec. IV A of Ref. [15]), and $\tau = \mu/\gamma$ for TDGL-C; $\omega = \sqrt{\omega_A^2 - \gamma^2/4}$ is the effective vibrational frequency, with ω_A as the characteristic frequency of polarization near P_A , i.e., $\omega_A = \sqrt{\partial_i^2 U/\mu}$. Without the inertial term of $\mu \ddot{P}$, the polarization P_i decays exponentially in TDGL-A, and $\langle P_i \rangle = P_0$ when the system is under equilibrium with $t \rightarrow \infty$. Otherwise, vibration is revealed because of the presence of $\cos(\omega t)$ induced by $\mu \ddot{P}$ in TDGL-C. With time elapsed, such vibration amplitude, i.e., $\Delta e^{-t/2\tau}$, decays and finally vanishes when the system reaches the equilibrium state with $t \rightarrow \infty$, so that $\langle P_i \rangle = P_0$ at the equilibrium state. In this regard, one can get the mathematical expectation $\langle P_i \rangle$ under the given potential field without the random force, and the inertial term gives rise to the thermal vibrations when the system relaxes to be equilibrium. On the other hand, the variance $\sigma_P^2(t)$ cannot

be maintained as $\sigma_P^2(t) \rightarrow 0$ under equilibrium with $t \rightarrow \infty$ because

$$\left\{ \begin{array}{l} \sigma_P^2(t) = \langle (P_i(t) - P_0)^2 \rangle = \Delta^2 e^{-t/\tau}, \\ \sigma_P^2(t) = \langle (P_i(t) - P_0)^2 \rangle = \Delta^2 e^{-t/\tau} \cos^2(\omega t), \end{array} \right. \quad (\text{D3})$$

which can be obtained according to Eq. (D2).

Let us check the above conclusion from another point of view.

(1) We multiply P_i to both sides of TDGL-A, and take the ensemble average, then we have

$$\langle P_i \dot{P}_i \rangle + \langle P_i \gamma \partial_i U \rangle = 0 \quad \Rightarrow \quad \frac{d\sigma_P^2}{dt} = -2\gamma k_B T_P(t), \quad (\text{D4})$$

where we define the time derivative of σ_P^2 as

$$\frac{d\sigma_P^2}{dt} = \frac{d}{dt} \langle P_i^2 \rangle - P_0^2 = \frac{d}{dt} \langle P_i^2 \rangle = 2 \langle P_i \dot{P}_i \rangle \quad (\text{D5})$$

and use the definition of $\langle P_i \partial_i U \rangle = k_B T_P(t)$. In principle, the thermodynamic temperature T_P could only be well defined when the system is under equilibrium. As discussed in Sec. II C, under the local equilibrium assumption [41,42], one can define the instantaneous temperature $T_P(t)$ as a thermodynamic observable, through the similar way as the one under equilibrium. According to statistic thermodynamics, when the system stays at the equilibrium states as $t \rightarrow \infty$, the probability distribution function ϱ is time independent, so are the macroscopic thermodynamic quantities. In particular, because the variance σ_P^2 is the second central moment of ϱ , we have $\sigma_P^2 = \text{const}$ when $t \rightarrow \infty$, and

$$\lim_{t \rightarrow \infty} \frac{d\sigma_P^2}{dt} = -2\gamma k_B \lim_{t \rightarrow \infty} T_P(t) = 0. \quad (\text{D6})$$

That is why the thermodynamic temperature T_P is revealed to be zero in TDGL-A under equilibrium. Note that, under the local equilibrium assumption and $\Delta \ll P_0$, the relation $\sigma_P^2(t) = \Omega^{-1} \chi k_B T_P(t)$ can be established by referring to Eq. (C9) [52], then we have $\sigma_P^2(t) \rightarrow 0$ as $t \rightarrow \infty$, which is consistent with Eq. (D3). More precisely, using $\tau = \chi/(2\gamma\Omega)$, Eq. (D4) can be derived as

$$\frac{dT_P}{dt} = -\frac{1}{\tau} T_P(t) \quad \text{or} \quad \frac{d\sigma_P^2}{dt} = -\frac{1}{\tau} \sigma_P^2(t). \quad (\text{D7})$$

Therefore,

$$T_P(t) = T_P^0 e^{-t/\tau} \quad \text{or} \quad \sigma_P^2(t) = \Delta^2 e^{-t/\tau}. \quad (\text{D8})$$

Here, T_P^0 is the initial value of T_P associated with the value of Δ or $\langle P_i \partial_i U \rangle$ at $t = 0$. Equation (D8) is consistent with Eq. (D3), and the variance σ_P^2 characterized the thermodynamic temperature of polarization dynamics.

Otherwise, applying the similar mathematical process to TDGL-B, we can have

$$\langle P_i \dot{P}_i \rangle + \langle P_i \gamma \partial_i U \rangle = \langle P_i \xi_i \rangle \Rightarrow \frac{d\sigma_P^2}{dt} = -2\gamma k_B [T_P(t) - T_x]. \quad (\text{D9})$$

Here, T_x is the temperature of the heat bath for the polarization dynamics provided by the DOF of $\{x_j\}$. The calculation of $\langle P_i \xi_i \rangle = \gamma k_B T_x$ follows the Furutsu-Novikov theorem (FNT) [61,62]. In FNT, if there is a thermodynamic quantity A that is the functional of the Gaussian random force $\xi(t)$ as

$A(t) = A[\xi(t)]$, the ensemble average of the product of $A(t)$ and $\xi(t)$ equals

$$\langle A(t)\xi(t) \rangle = \int dt' \left(\langle \xi(t)\xi(t') \rangle \left\langle \frac{\delta A(t)}{\delta \xi(t')} \right\rangle \right) \quad (\text{D10})$$

with $\delta A(t)/\delta \xi(t')$ the functional derivative. Because

$$\langle \xi(t)\xi(t') \rangle = 2\gamma k_B T_x \delta(t-t') \quad (\text{D11})$$

we have

$$\langle A(t)\xi(t) \rangle = 2\gamma k_B T_x \left\langle \frac{\delta A(t)}{\delta \xi(t)} \right\rangle. \quad (\text{D12})$$

Replacing $A(t)$ by $P_i(t)$ in Eq. (D12), we can get

$$\langle P_i \xi_i \rangle = 2\gamma k_B T_x \left\langle \frac{\delta P_i(t)}{\delta \xi_i(t)} \right\rangle. \quad (\text{D13})$$

According to the TDGL-B,

$$P_i(t) = P_i(0) + \int_0^t d\tau [-\gamma \partial_i U + \xi_i(\tau)]. \quad (\text{D14})$$

Following Eq. (36) in Ref. [61], we have

$$\frac{\delta P_i(t)}{\delta \xi_i(t)} = \frac{1}{2} \Rightarrow \langle P_i \xi_i \rangle = \gamma k_B T_x. \quad (\text{D15})$$

Tracing back to Eq. (D6), when $t \rightarrow \infty$, the thermodynamic requirement of $\sigma_P^2 = \text{const}$ results in

$$\lim_{t \rightarrow \infty} \frac{d\sigma_P^2}{dt} = -2\gamma k_B \lim_{t \rightarrow \infty} [T_P(t) - T_x] = 0 \Rightarrow \lim_{t \rightarrow \infty} T_P(t) = T_x, \quad (\text{D16})$$

where the thermodynamic zeroth law, once again, is satisfied.

Similar to the deduction of Eq. (D7), Eq. (D16) can be also derived as

$$\frac{dT_P}{dt} = -\frac{1}{\tau} [T_P(t) - T_x] \quad (\text{D17})$$

whose solution is then given by

$$\sigma_P^2(t) \propto T_P(t) = T_x + (T_P^0 - T_x)e^{-t/\tau}. \quad (\text{D18})$$

In this regard, as long as $T_x \neq 0$, the variance of σ_P^2 will always be existing because of $\sigma_P^2(t) \propto T_P(t)$. In addition, we can see in Eq. (D6) the actions of random force $\xi_i(t)$ and the dissipation $-\gamma \partial_i U$, respectively, correspond to the thermodynamic temperature of heat bath T_x and polarization T_P , both of which are balanced when the system is under equilibrium as $t \rightarrow \infty$. Again, comparing with Eqs. (D4) and (D6), that is why the presence of random force, together with the dissipation, guarantees the thermodynamics and microdynamics of polarization dynamics in PFM simulations. Therefore, the random force and dissipation term are the entirety of the thermodynamic environment.

(2) We multiply \dot{P}_i to TDGL-C, and take the ensemble average, then we have

$$\begin{aligned} \langle \dot{P}_i \mu \ddot{P}_i \rangle + \langle \dot{P}_i \gamma \dot{P}_i \rangle + \langle \dot{P}_i \partial_i U \rangle &= 0 \\ \Rightarrow \frac{d}{dt} \left\langle \frac{1}{2} \mu \dot{P}_i^2 \right\rangle + \frac{\gamma}{\mu} \langle \mu \dot{P}_i^2 \rangle + \frac{d}{dt} \langle U \rangle &= 0. \end{aligned} \quad (\text{D19})$$

If we define the total ‘‘mechanical’’ energy E_{tot} of polarization dynamics as $E_{\text{tot}} = E_K + E_P$, with E_K and E_P as the kinetic

and potential energies, respectively, as

$$E_K = \left\langle \frac{1}{2} \mu \dot{P}_i^2 \right\rangle \quad \text{and} \quad E_P = \langle U \rangle \quad (\text{D20})$$

and using the definition of $k_B T_P(t) = \langle \mu \dot{P}_i^2 \rangle$, we have

$$\frac{dE_{\text{tot}}}{dt} = -\frac{\gamma}{\mu} k_B T_P(t). \quad (\text{D21})$$

With the thermodynamic requirement of $E_{\text{tot}} = \text{const}$ under equilibrium when $t \rightarrow \infty$, we have

$$\lim_{t \rightarrow \infty} \frac{dE_{\text{tot}}}{dt} = -\frac{\gamma}{\mu} k_B \lim_{t \rightarrow \infty} T_P(t) = 0. \quad (\text{D22})$$

Therefore, the introduction of the inertial term of $\mu \ddot{P}_i$ into the TDGL-A, i.e., TDGL-C, cannot prevent the thermodynamic temperature T_P from approaching zero, and the thermodynamic zeroth law cannot be held. It could only give rise to the energetic exchange between the kinetic and potential energies [see Eq. (D19) or (D21)] during the system approaching its equilibrium state, accompanying with the decayed oscillations of observed [see Eqs. (D2) and (D3)].

Applying similar mathematical process to TDGL-D, we can have

$$\langle \dot{P}_i \mu \ddot{P}_i \rangle + \langle \dot{P}_i \gamma \dot{P}_i \rangle + \langle \dot{P}_i \partial_i U \rangle = \langle \dot{P}_i \xi_i \rangle. \quad (\text{D23})$$

Similar to the deduction of Eq. (D19), we have

$$\frac{dE_{\text{tot}}}{dt} = -\frac{\gamma}{\mu} k_B [T_P(t) - T_x]. \quad (\text{D24})$$

Here, the relation of

$$\langle \dot{P}_i \xi_i \rangle = \frac{\gamma}{\mu} k_B T_x \quad (\text{D25})$$

can be obtained similar to that in Eq. (D12). Replacing $A(t)$ by $\dot{P}_i(t)$ in Eq. (D12), we can get

$$\langle \dot{P}_i \xi_i \rangle = 2\gamma k_B T_x \left\langle \frac{\delta \dot{P}_i(t)}{\delta \xi_i(t)} \right\rangle. \quad (\text{D26})$$

According to TDGL-D,

$$\dot{P}_i(t) = \dot{P}_i(0) + \frac{1}{\mu} \int_0^t d\tau (-\gamma \dot{P}_i - \partial_i U + \xi_i(\tau)) \quad (\text{D27})$$

and we have

$$\frac{\delta \dot{P}_i(t)}{\delta \xi_i(t)} = \frac{1}{2\mu} \quad (\text{D28})$$

referring to Eq. (36) in Ref. [61]. Finally, substituting Eq. (D28) into (D26), we can get the relation of Eq. (D25). Following Eq. (D24), the same thermodynamic requirement of $E_{\text{tot}} = \text{const}$ as $t \rightarrow \infty$ leads to

$$\lim_{t \rightarrow \infty} \frac{dE_{\text{tot}}}{dt} = -\frac{\gamma}{\mu} k_B \lim_{t \rightarrow \infty} [T_P(t) - T_x] = 0 \quad (\text{D29})$$

so that

$$\lim_{t \rightarrow \infty} T_P(t) = T_x, \quad (\text{D30})$$

indicating that the thermodynamic zeroth law is satisfied. As we can see in Eq. (D30), the actions of random force $\xi_i(t)$ and the dissipation $-\gamma \dot{P}_i$ in TDGL-D, respectively,

correspond to the thermodynamic temperature of heat bath T_x and polarization T_p , both of which together constitute the thermodynamic environment. In particular, these two actions are balanced when the system reaches its equilibrium state with $t \rightarrow \infty$, guaranteeing the thermodynamic zeroth law.

To sum up, we can conclude that (1) given the appropriate potential field U , the mathematical expectation $\langle P_i \rangle$ can be well reproduced by the TDGL equation, whether the effects of random force are taken into account or not. (2) The random

force $\xi_i(t)$ and the dissipation terms, either $-\gamma \partial_i U$ or $-\gamma \dot{P}_i$, are the entirety of the thermodynamic environment, both of which guarantee the thermodynamic zeroth law. In particular, the variance $\langle P_i^2 \rangle \neq 0$ could be only existing by accounting for the effects of random force. (3) The inertial term can result in the thermal vibrations when the system relaxes to be equilibrium, but such vibrations will vanish as it reaches the equilibrium states without the actions of random force. In this regard, the actions of random force and inertial term could not be treated as the simple accumulation.

-
- [1] T. Qi, Y.-H. Shin, K.-L. Yeh, K. A. Nelson, and A. M. Rappe, Collective Coherent Control: Synchronization of Polarization in Ferroelectric PbTiO₃ by Shaped THz Fields, *Phys. Rev. Lett.* **102**, 247603 (2009).
- [2] Y. Zheng and W. J. Chen, Characteristics and controllability of vortices in ferromagnetics, ferroelectrics, and multiferroics, *Rep. Prog. Phys.* **80**, 086501 (2017).
- [3] R. Mankowsky, A. von Hoegen, M. Först, and A. Cavalleri, Ultrafast Reversal of the Ferroelectric Polarization, *Phys. Rev. Lett.* **118**, 197601 (2017).
- [4] Z. Gu, S. Pandya, A. Samanta, S. Liu, G. Xiao, C. J. Meyers, A. R. Damodaran, H. Barak, A. Dasgupta, S. Saremi, A. Polemi, L. Wu, A. A. Podpirka, A. Will-Cole, C. J. Hawley, P. K. Davies, R. A. York, I. Grinberg, L. W. Martin, and J. E. Spanier, Resonant domain-wall-enhanced tunable microwave ferroelectrics, *Nature (London)* **560**, 622 (2018).
- [5] J. Liu, Y. Ji, S. Yuan, L. Ding, W. Chen, and Y. Zheng, Controlling polar-toroidal multi-order states in twisted ferroelectric nanowires, *npj Comput. Mater.* **4**, 78 (2018).
- [6] C. Paillard, E. Torun, L. Wirtz, J. Íñiguez, and L. Bellaiche, Photoinduced Phase Transitions in Ferroelectrics, *Phys. Rev. Lett.* **123**, 087601 (2019).
- [7] C. Elissalde and J. Ravez, Ferroelectric ceramics: Defects and dielectric relaxations, *J. Mater. Chem.* **11**, 1957 (2001).
- [8] J. Y. Jo, S. M. Yang, T. H. Kim, H. N. Lee, J.-G. Yoon, S. Park, Y. Jo, M. H. Jung, and T. W. Noh, Nonlinear Dynamics of Domain-Wall Propagation in Epitaxial Ferroelectric Thin Films, *Phys. Rev. Lett.* **102**, 045701 (2009).
- [9] C. M. Fancher, S. Brewer, C. C. Chung, S. Röhrig, T. Rojac, G. Esteves, M. Deluca, N. Bassiri-Gharb, and J. L. Jones, The contribution of 180° domain wall motion to dielectric properties quantified from in situ X-ray diffraction, *Acta Mater.* **126**, 36 (2017).
- [10] M. Sepiarsky, S. R. Phillpot, S. K. Streiffer, M. G. Stachiotti, and R. L. Migoni, Polarization reversal in a perovskite ferroelectric by molecular-dynamics simulation, *Appl. Phys. Lett.* **79**, 4417 (2001).
- [11] Y. H. Shin, I. Grinberg, I. W. Chen, and A. M. Rappe, Nucleation and growth mechanism of ferroelectric domain-wall motion, *Nature (London)* **449**, 881 (2007).
- [12] I. Grinberg, Y.-H. Shin, and A. M. Rappe, Molecular Dynamics Study of Dielectric Response in a Relaxor Ferroelectric, *Phys. Rev. Lett.* **103**, 197601 (2009).
- [13] S. Liu, I. Grinberg, and A. M. Rappe, Intrinsic ferroelectric switching from first principles, *Nature (London)* **534**, 360 (2016).
- [14] V. Boddu, F. Endres, and P. Steinmann, Molecular dynamics study of ferroelectric domain nucleation and domain switching dynamics, *Sci. Rep.* **7**, 806 (2017).
- [15] J. Liu, H. Wen, W. Chen, and Y. Zheng, Atomistic studies of temporal characteristics of polarization relaxation in ferroelectrics, *Phys. Rev. B* **103**, 014308 (2021).
- [16] T. Nishimatsu, U. V. Waghmare, Y. Kawazoe, and D. Vanderbilt, Fast molecular-dynamics simulation for ferroelectric thin-film capacitors using a first-principles effective Hamiltonian, *Phys. Rev. B* **78**, 104104 (2008).
- [17] S. Lisenkov, I. Ponomareva, and L. Bellaiche, Unusual static and dynamical characteristics of domain evolution in ferroelectric superlattices, *Phys. Rev. B* **79**, 024101 (2009).
- [18] Q. Zhang, R. Herchig, and I. Ponomareva, Nanodynamics of Ferroelectric Ultrathin Films, *Phys. Rev. Lett.* **107**, 177601 (2011).
- [19] L.-Q. Chen, Phase-field method of phase transitions/domain structures in ferroelectric thin films: A review, *J. Am. Ceram. Soc.* **91**, 1835 (2008).
- [20] J.-J. Wang, B. Wang, and L.-Q. Chen, Understanding, predicting, and designing ferroelectric domain structures and switching guided by the phase-field method, *Annu. Rev. Mater. Res.* **49**, 127 (2019).
- [21] L.-Q. Chen and Y. Zhao, From classical thermodynamics to phase-field method, *Prog. Mater. Sci.* **124**, 100868 (2022).
- [22] H. Akamatsu, Y. Yuan, V. A. Stoica, G. Stone, T. Yang, Z. Hong, S. Lei, Y. Zhu, R. C. Haislmaier, J. W. Freeland, L.-Q. Chen, H. Wen, and V. Gopalan, Light-Activated Gigahertz Ferroelectric Domain Dynamics, *Phys. Rev. Lett.* **120**, 096101 (2018).
- [23] T. Yang, B. Wang, J.-M. Hu, and L.-Q. Chen, Domain Dynamics under Ultrafast Electric-Field Pulses, *Phys. Rev. Lett.* **124**, 107601 (2020).
- [24] R. Indergand, A. Vidyasagar, N. Nadkarni, and D. M. Kochmann, A phase-field approach to studying the temperature-dependent ferroelectric response of bulk polycrystalline PZT, *J. Mech. Phys. Solids* **144**, 104098 (2020).
- [25] J. S. Rowlinson, Translation of J. D. van der Waals' "The thermodynamik theory of capillarity under the hypothesis of a continuous variation of density", *J. Stat. Phys.* **20**, 197 (1979).
- [26] W. Cao and L. E. Cross, Theory of tetragonal twin structures in ferroelectric perovskites with a first-order phase transition, *Phys. Rev. B* **44**, 5 (1991).
- [27] S. Nambu and D. A. Sagala, Domain formation and elastic long-range interaction in ferroelectric perovskites, *Phys. Rev. B* **50**, 5838 (1994).

- [28] H. L. Hu and L.-Q. Chen, Computer simulation of 90° ferroelectric domain formation in two-dimensions, *Mater. Sci. Eng. A* **238**, 182 (1997).
- [29] H. L. Hu and L.-Q. Chen, Three-dimensional computer simulation of ferroelectric domain formation, *J. Am. Ceram. Soc.* **81**, 492 (1998).
- [30] P. C. Hohenberg and B. I. Halperin, Theory of dynamic critical phenomena, *Rev. Mod. Phys.* **49**, 435 (1977).
- [31] J. D. Gunton, M. San Miguel, and P. S. Sahni, in *Phase Transitions and Critical Phenomena*, Vol. 8, edited by C. Domb and J. L. Lebowitz (Academic, New York, 1983), pp. 267–466
- [32] J. Rolland, F. Bouchet, and E. Simonnet, Computing transition rates for the 1-D stochastic Ginzburg-Landau-Allen-Cahn equation for finite-amplitude noise with a rare event algorithm, *J. Stat. Phys.* **162**, 277 (2016).
- [33] G. Geneste, L. Bellaïche, and J.-M. Kiat, Simulating the Radio-Frequency Dielectric Response of Relaxor Ferroelectrics: Combination of Coarse-Grained Hamiltonians and Kinetic Monte Carlo Simulations, *Phys. Rev. Lett.* **116**, 247601 (2016).
- [34] C. H. Woo, H. Wen, A. A. Semenov, S. L. Dudarev, and P.-W. Ma, Quantum heat bath for spin-lattice dynamics, *Phys. Rev. B* **91**, 104306 (2015).
- [35] J. O. Hirschfelder, Classical and quantum mechanical hypervirial theorems, *J. Chem. Phys.* **33**, 1462 (1960).
- [36] H. H. Rugh, Dynamical Approach to Temperature, *Phys. Rev. Lett.* **78**, 772 (1997).
- [37] O. G. Jepps, G. Ayton, and D. J. Evans, Microscopic expressions for the thermodynamic temperature, *Phys. Rev. E* **62**, 4757 (2000).
- [38] J. G. Powles, G. Rickayzen, and D. M. Heyes, Temperatures: Old, new and middle aged, *Mol. Phys.* **103**, 1361 (2005).
- [39] S. Davis and G. Gutiérrez, Conjugate variables in continuous maximum-entropy inference, *Phys. Rev. E* **86**, 051136 (2012).
- [40] A. Puglisi, A. Sarracino, and A. Vulpiani, Temperature in and out of equilibrium: A review of concepts, tools and attempts, *Phys. Rep.* **709–710**, 1 (2017).
- [41] J. Casas-Vázquez and D. Jou, Nonequilibrium temperature versus local-equilibrium temperature, *Phys. Rev. E* **49**, 1040 (1994).
- [42] J. Casas-Vázquez and D. Jou, Temperature in non-equilibrium states: a review of open problems and current proposals, *Rep. Prog. Phys.* **66**, 1937 (2003).
- [43] A. K. Bandyopadhyay, P. C. Ray, and V. Gopalan, An approach to the Klein-Gordon equation for a dynamic study in ferroelectric materials, *J. Phys.: Condens. Matter* **18**, 4093 (2006).
- [44] Y. L. Li, L. E. Cross, and L. Q. Chen, A phenomenological thermodynamic potential for BaTiO₃ single crystals, *J. Appl. Phys.* **98**, 064101 (2005).
- [45] W. Chen, J. Liu, L. Ma, L. Liu, G. Jiang, and Y. Zheng, Mechanical switching of ferroelectric domains beyond flexoelectricity, *J. Mech. Phys. Solids* **111**, 43 (2018).
- [46] A. K. Tagantsev, L. E. Cross, and J. Fousek, Switching phenomena and small-signal response, *Domains in Ferroic Crystals and Thin Films* (Springer, New York, 2010), pp. 351–519.
- [47] S. Boyn, J. Grollier, G. Lecerf, B. Xu, N. Locatelli, S. Fusil, S. Girod, C. Carrétéro, K. Garcia, S. Xavier, J. Tomas, L. Bellaïche, M. Bibes, A. Barthélémy, S. Saighi, and V. Garcia, Learning through ferroelectric domain dynamics in solid-state synapses, *Nat. Commun.* **8**, 14736 (2017).
- [48] Y. L. Li, S. Y. Hu, Z. K. Liu, and L. Q. Chen, Phase-field model of domain structures in ferroelectric thin films, *Appl. Phys. Lett.* **78**, 3878 (2001).
- [49] Y. Gu, Z. Hong, J. Britson, and L.-Q. Chen, Nanoscale mechanical switching of ferroelectric polarization via flexoelectricity, *Appl. Phys. Lett.* **106**, 022904 (2015).
- [50] W. Xiong, J. Liu, L. Ma, W. Chen, and Y. Zheng, Tip-force-induced ultrafast polarization switching in ferroelectric thin film: A dynamical phase field simulation, *J. Appl. Phys.* **128**, 014102 (2020).
- [51] H. A. Kramers, Brownian motion in a field of force and the diffusion model of chemical reactions, *Physica (Amsterdam)* **7**, 284 (1940).
- [52] T. Hashimoto and H. Moriwake, Dielectric properties of BaTiO₃ by molecular dynamics simulations using a shell model, *Mol. Simul.* **41**, 1074 (2015).
- [53] S. Prosandeev, I. Ponomareva, I. Naumov, I. Kornev, and L. Bellaïche, Original properties of dipole vortices in zero-dimensional ferroelectrics, *J. Phys.: Condens. Matter* **20**, 193201 (2008).
- [54] K. Lai, H. Wen, J. Liu, Y. Wu, and Y. Zheng, Ferromagnetic effects on non-Arrhenius diffusion of single interstitial helium solute in BCC Fe, *J. Nucl. Mater.* **524**, 286 (2019).
- [55] Y. Wu, H. Wen, W. Chen, and Y. Zheng, Microdynamic Study of Spin-Lattice Coupling Effects on Skyrmion Transport, *Phys. Rev. Lett.* **127**, 097201 (2021).
- [56] Q. Li, V. A. Stoica, M. Paściak, Y. Zhu, Y. Yuan, T. Yang, M. R. McCarter, S. Das, A. K. Yadav, S. Park, C. Dai, H. J. Lee, Y. Ahn, S. D. Marks, S. Yu, C. Kadlec, T. Sato, M. C. Hoffmann, M. Chollet, M. E. Kozina *et al.*, and Subterahertz collective dynamics of polar vortices, *Nature (London)* **592**, 376 (2021).
- [57] M. G. Guenza, Structural and thermodynamic consistency in coarse-grained models of macromolecules, *J. Phys.: Conf. Ser.* **640**, 012009 (2015).
- [58] Y. Zheng and C. H. Woo, Thermodynamic modeling of critical properties of ferroelectric superlattices in nano-scale, *Appl. Phys. A* **97**, 617 (2009).
- [59] A. K. Tagantsev, L. E. Cross, and J. Fousek, Fundamentals of ferroic domain structures, *Domains in Ferroic Crystals and Thin Films* (Springer, New York, 2010), pp. 11–107.
- [60] A. P. Levanyuk, B. A. Strukov, and A. Cano, Background dielectric permittivity: Material constant or fitting parameter? *Ferroelectrics* **503**, 94 (2016).
- [61] R. F. Fox, Functional-calculus approach to stochastic differential equations, *Phys. Rev. A* **33**, 467 (1986).
- [62] P.-W. Ma and S. L. Dudarev, Langevin spin dynamics, *Phys. Rev. B* **83**, 134418 (2011).